CHAPTER VI
MISCIBILITY, MELTING, CRYSTALLIZATION KINETICS BEHAVIORS, AND MORPHOLOGIES OF PTT/PEN BLENDS

ABSTRACT

Blends of poly(trimethylene terephthalate) (PTT) and poly(ethylene 2,6-naphthalate) in the amorphous state were miscible in all of the blend compositioins studied, as evidenced by a single, composition-dependent glass-transition temperature observed for each blend composition. The variation in the glass-transition temperature was well-predicted by the Gordon-Taylor equation, with the fitting parameter being 1.1554. The cold-crystallization (peak) temperature increased with increasing PEN content in the blends. The subsequent melting endotherms after melt crystallization exhibited melting point depression behavior in which the observed melting temperatures decreased with an increasing amount of minor component of the blends. LHW and NLHW were used to determine the equilibrium melting temperature of the blends. The values of the overall crystallization rate parameters for these blends were all found to increase with decreasing crystallization temperature, suggesting that these blends crystallized at low temperatures faster than that at high temperatures. Considering at the same T_c, the $t_{0.5}^{-1}$, K_a, C_1, and K_{us} values of 97PTT/3PEN are greater than those of pure PTT. As the content of PEN was further increased to 6 and 9 % wt, these values dramatically decreased. This result is similar to that observed in the growth rate. For a same undercooling, the spherulite growth rate of the blends is higher than that of pure PTT whereas spherulite growth rates in the blends are unaffected by composition in range studied. From LH secondary nucleation theory, PTT and 91PTT/9PEN showed the transition temperatures between regime III and II about 194°C while those of 97PTT/3PEN and 94PTT/6PEN could not observed from this crystallization temperature T_c range studied. However, the regime growth of 97PTT/3PEN and 94PTT/6PEN was found to be regime II for crystallization temperature range studied. Banded spherulites were observed for PTT/PEN blends. The spacing of bands of PTT increases with increasing T_c. The body of spherulite

texture is more open with increasing PEN content. In addition, the boundary of spherulite is also changed with composition.

(**Key-words:** poly(trimethylene terephthalate); poly(ethylene 2,6-naphthalate); crystallization; banded spherulite)

1. INTRODUCTION

Poly(trimethylene terephthalate) (PTT) as semicrystalline polymer is a linear aromatic polyester which was firstly synthesized by Whinfield and Dickson in 1941 [1]. But it was not commercially available due to the high cost of 1,3 propanediol (PDO), one of raw materials that are used for producing PTT. However, recent breakthroughs in PDO synthesis via hydroformylation of ethylene oxide, process improvements in traditional synthetic route through acrolein and promising bioengineering route have reduced the cost of PDO [2]. These bring PTT become commercial polymer, joining the other aromatic polyesters, poly(ethylene terephthalate) (PET), and poly(buthylene terephthalate) (PBT). It can be used in many applications such as fibers, films, and engineering thermoplastics. Mechanical properties of PTT are roughly between those of PET and PBT. Of interest is that PTT had a better tensile elastic recovery and a lower modulus than PET and PBT [3].

Nowadays, polymer blends are the great interesting scientific study [4-11]. There are physical mixtures of structurally different polymers, which adhere together through the interaction of secondary bond forces, with no covalent bonding between them [4]. In the search for new polymeric materials, blending of polymers is a method for obtaining new desirable property combinations without having to synthesize novel structures. Generally, the final properties of blends are strongly dependent on the developed crystallinity and morphology, occurring during the processing. In addition, the miscibility of components also affects the final properties of the blends. In order to ensure high temperature and environmental resistance, the high performance thermoplastics are usually characterized by a certain degree of crystallinity. Therefore, it is of interest to understand the miscibility of polymer blends containing at least one component capable of crystallizing [4].

Numerous published articles related to various aspects of binary blends of polyesters are available in the open literature. Some of these are, for examples, blends of PET and PBT [4], PBT and an amorphous co-polyester of cyclohexane dimethanol, ethylene glycol, and terephthalic acid (PETG) [5], and PET and poly(ethylene 2,6-naphthalate) (PEN) [6]. Recently, PTT-blends systems have been studied extensively (e.g., the blends of PTT and PET [7]; of PTT and PBT [8,9]; of PTT and poly(ether imide) (PEI) [10]). However, the blends of PTT and PEN, to best of our knowledge, have not yet been available.

The aim of this work is to investigate the miscibility, melting behavior, overall and growth crystallization kinetics, and morphology of the blends of PTT and PEN at low PEN content.

2. EXPERIMENTAL

2.1 Material

Poly(trimethylene terephthalate) (PTT) was supplied in pellet form by Shell Chemicals Company (USA) (Corterra CP509201). The weight- and number-average molecular weights of this resin were determined to be ca. 78,100 and 34,700 Daltons, respectively. Molecular weight characterization was carried out by size-exclusion chromatography (SEC). Poly(ethylene 2,6-naphthalate) (PEN) was supplied in pellet form by BP Chemicals Company (USA)

2.2 Samples Preparation

PTT and PEN pallets were dried in a vacuum oven at 140°C for 5 hours and then were pre-mixed in a dry mixer to produce PTT/PEN pre-blends of 3, 6, 9 % wt of PEN, respectively. The pre-blends were then melt-mixed in a self-wiping, co-rotating twin-screw extruder (Collin, ZK 25), operating at a screw speed of 40 rpm and using extrusion temperature of 150, 270, 280, 290, 300, 280°C for Feeding Zone, Zone 1, Zone 2, Zone 3, Zone 4, Die, respectively. The extrudate were cooled in water and were pelletized using a pelletizer (Planetrol, 075D2). The resulting blends were hereafter denoted (1-x)PTT/xPEN, where x is the weight percentage of PEN in blends. Films of approximately 200 μm thickness for neat resins and their blends were obtained by melt-pressing at 300°C in a compression molding machine

(Wabash V50H) under an applied pressure of 3 ton-force. After 2 min holding time, the films were removed and allowed to cool down to room temperature, under the ambient condition, between the two metal platens. This treatment assumes that the previous thermo-mechanical history was essentially erased and provides a standard crystalline memory condition for our experiments

2.3 Differential Scannig Calorimetry Measurements

In this study, a Perkin-Elmer Series 7 DSC (DSC-7) was used to observe glass transition temperatures, equilibrium melting temperatures and study the overall crystallization kinetics of isothermally melt-crystallized PTT, PEN and their blends. Temperature calibration was carried out using an indium standard (T_m^o = 156.6°C and ΔH_f^o = 28.5 J g^{-1}). The consistency of the temperature calibration was checked every other run to ensure the reliability of the data obtained. To minimize thermal lag between polymer sample and DSC furnace, each sample holder was loaded with a disc-shape sample, weighing around 8.0 ± 0.5 mg, which was cut from the prepared films. It is worth noting that each sample was used only once and all the runs were preformed under nitrogen atmosphere to prevent extensive thermal degradation.

For the glass transition temperature (T_g) measurement, the experiment started with heating PTT, PEN and their blends from 30°C to a fusion temperature of 300°C at a heating rate 80°C min^{-1} for a melt-annealing period of 5 min in order to remove previous thermal histories, after which the samples were taken out and immediately quenched in liquid nitrogen to attain the completely amorphous state of the samples. In order to observe the glass transition temperature, each sample was reheated again in DSC from 25 to 300°C at a rate of 10°C min^{-1}. For the study of overall isothermal crystallization from the melt state, the experiment started with heating PTT and the blends from 30°C at a heating rate of 80°C min^{-1} to 300°C, where it was held for 5 min to ensure complete melting. After this period, each sample was rapidly cooled (i.e., at a cooling rate 200°C min^{-1}) to a desired crystallization temperature T_c ranging from 190 to 205°C (in case of PEN samples, they were crystallized isothermally between 237.5 and 250°C), where it was held until crystallization process was consider complete (when no significant change in

the heat flow as a function of time was further observed). The crystallization exotherm was recorded for analysis with Avrami, Malkin and Urbanovici-Segal macrokinetic model. Then the sample was heated with a constant scanning rate of $10^{o}C\ min^{-1}$ to observe the subsequent melting endotherm, where the melting temperature of isothermally crystallized samples were recorded to calculate equilibrium melting temperatures based on the Hoffman-Weeks theory.

2.4 Morphology and Spherulite Growth Rate Measurements

The morphology and radius growth of PTT and the blends crystallite under isothermal crystallization were investigated using a polarized light microscope (Leica DMRXP) equipped with a hot stage (Mettler Toledo FP82HT), a temperature control system (Mettler Toledo FP90), and a CCD camera (Cohu 4910). Specimen was prepared by melting the sample on a glass slide on a hot stage at 300°C, followed by pressing of the melted sample with a piece of cover glass and maintained for 5 min at this temperature to remove previous thermal history. Then the specimen was rapidly transferred to another hot stage which lies on the stage of polarized light microscope and the temperature was already set at desired crystallization temperature ranging from 185 to 210°C. The subsequent growth of particularly selected spherulite was viewed between crossed polars and recorded by a CCD camera at appropriate time intervals. The images of spherulitic radius were analyzed on a computer using the Scion image software. By plotting spherulite radius as a function of time, the slope of the line or the spherulite growth rate at desired crystallization temperature ranging from 185 to 210°C were obtained.

3. RESULTS AND DISCUSSION

3.1 Glass Transition Temperature

Differential scanning calorimetry has been extensively used to investigate miscibility in polymer blends. Figure 1 shows DSC traces for quenched PTT, PEN and PTT/PEN blends at a heating rate of $10^{o}C\ min^{-1}$. Essentially only one T_g was observed for all compositions in this studied range, and was located between T_g of the pure components (i.e., $T_{g,PTT}$ = 39.206°C and $T_{g,PEN}$ = 118.601°C). As clearly observed, the T_g rises monotonically with increasing PEN content in the blends,

indicating miscibility between two polymer in the amorphous state. The T_g values of PTT, 97PTT/3PEN, 94PTT/6PEN, 91PTT/9PEN, and PEN are 39.206, 42.282, 45.536, 46.134, and 118.601°C, respectively. Moreover, the cold-crystallization temperature T_{cc} increases with increasing PEN content, as shown in Figure 1. This result implies that the presence of PEN retards PTT crystallization from the glassy state.

For a miscible polymer blend system, a number of empirical models have been proposed to predict the composition-dependence of T_g of the blend. One of the most widely used models is the Fox equation. In this model, the observed T_g value of the blend relates to the glass transition temperatures of the pure components 1 and 2 (i.e., T_{g1} and T_{g2}) and the blend composition according to the following equation [12]:

$$\frac{1}{T_g} = \frac{w_1}{T_{g1}} + \frac{w_2}{T_{g2}} \quad , \tag{1}$$

where w_1 and w_2 are the weight fractions (in the amorphous state only) of components 1 and 2, respectively, and T_{g1} and T_{g2} are respective T_g values of the pure components 1 and 2.

The Fox equation assumes random mixing between the two components, equal values of the enthalpic jump in the glass transition region between the two components (i.e., $\Delta C_{p1} = \Delta C_{p2}$), and no volume expansion between the two components during mixing. The dependence of the T_g value on the blend composition for PTT/PEN blends is illustrated in Figure 2. The dotted line is the predicted composition-dependence of the T_g value for PTT/PEN blends according to the Fox equation. Apparently, the experimental T_g values of the blends are higher than those calculated by the Fox equation.

Another popular equation used to predict composition-dependent behavior of T_g for a miscible polymer blend is the Gordon-Taylor equation [13], which can be written as:

$$T_g = \frac{w_1 T_{g1} + k w_2 T_{g2}}{w_1 + k w_2} \quad , \tag{2}$$

where k is an adjustable parameter. The solid line shown in Figure 2 is the predicted composition-dependence of the T_g value for PTT/PEN blends according to the Gordon-Taylor equation, with the fitting k parameter being 1.1554. Based on the predicted curve and the data shown in Figure 2, good agreement between the observed T_g values and the prediction by the Gordon-Taylor equation was obtained for blends in this studied range.

3.2 Melting Behavior

To determine the equilibrium melting temperature of PTT, PEN and their blends, it is necessary to understand the melting behaviors of the polymers. For PTT and the blends were isothermally crystallized at various crystallization temperatures T_c ranging from 190 to 205°C (in case of PEN samples, they were crystallized isothermally between 237.5-250°C) in a step increment of 2.5°C to examine the change of the multiple melting peaks. The melt-crystallized PTT, PEN and their blends were then scanned in DSC all at the same heating rate of 10°C min^{-1}. Figure 3 shows the subsequent melting endotherms for PTT, PEN and their blends isothermally crystallized from the melt state at various crystallization temperatures as indicated on the respective traces.

According to Figure 3(a), the subsequent melting endotherm for neat PTT exhibited triple (for T_c's lower than ≈ 195°C), or double (for T_c's greater than ≈ 195°C) endothermic melting phenomena. These endothermic peaks were labeled as peaks I, II, and III for low-, middle-, high-temperature melting endotherms, respectively [14]. For the triple melting phenomenon of PTT, it was postulated that the occurrence of peak I was a resulting of the melting of the primary crystallites, peak II was a result of the melting of recrystallized crystallites, and peak III was a result of the melting of the recrystallized crystallites of different stabilities [14]. Qualitatively, the position of peak I shifts towards a higher temperature with increasing T_c, while those of peaks II and III do not shift so much with increasing T_c. This observation was also found in PTT/PEN blends, as shown in Figure 3(b)-3(d). However, the composition of the blends affects on the multiple melting peaks when crystallized at the same range of crystallization temperatures. In case of 97PTT/3PEN, the subsequent melting endotherm exhibited triple endothermic

melting phenomena for T_c's lower than ≈ 195°C, double endothermic melting phenomena for T_c's greater than ≈ 195°C. This observation is similar to that of neat PTT. In case of 94PTT/6PEN and 91PTT/9PEN, the subsequent melting endotherm exhibited triple endothermic melting phenomena for T_c's lower than ≈ 192.5°C, double endothermic melting phenomena for T_c's greater than ≈ 192.5°C. In addition, the difference between neat PTT and the blends is the peak locations. At the same crystallization temperature, the melting peaks were systematically shifted toward lower temperatures with increasing PEN content, suggesting that the stability of PTT crystal decreases with increasing PEN content.

For the melting behavior of PEN, it also shows triple melting phenomena, which has been reported by Lee *et al.* [15]. The small and low-temperatue endotherm was postulated to be the melting of small crystallites formed between main lamellar populations, and the high-temperature endotherm was a result of the melting of crystallites produced by melt-recrystallization. The middle-temperature endotherm was attributed to be the melting of the original crystal lamellae grown formed at T_c. Figure 3(e) presents the subsequent melting endotherm for neat PEN exhibited double (for T_c's lower than ≈ 247.5°C), or single (for T_c's greater than ≈ 247.5°C) endothermic melting phenomena. These endothermic peaks were labeled as M, and H for middle-, and high-temperature endotherm, respectively. The position of middle-temperature endotherm increases with increasing T_c.

3.3 Determination of the Equilibrium Melting Temperature

As mention previously, the endothermic peak I (for neat PTT and the blends) and peak M (for neat PEN), which corresponded to the melting of primary crystal formed at a specified T_c; thus the T_I (for neat PTT and the blends) and T_M (for neat PEN) values listed in Table 1 are the observed T_m for determining the equilibrium melting temperature. According to a theory derived by Hoffman-Weeks [16], the equilibrium melting temperature T_m^o of a semicrystalline polymer can be estimated by a linear extrapolation of the observed T_m-T_c data to the line $T_m = T_c$. They arrived at the following equation, the linear Hoffman-Weeks extrapolation (LHW):

$$T_m = \frac{T_c}{2\beta} + T_m^o\left[1 - \frac{1}{2\beta}\right] \quad , \qquad (3)$$

where β is the thickening ratio. In other words, β indicates the ratio of the thickness of the mature crystal l_c to that of the initial one l_c^*; therefore, $\beta = l_c / l_c^*$, which is supposed to always be greater than or equal to one. The factor 2 in Equation (3) suggests that the thickness of the crystals undergoing melting is approximately double that of the initial critical thickness [17].

Figure 4(a)-4(e) illustrate the plots between the observed T_m and T_c for PTT, 97PTT/3PEN, 94PTT/6PEN, 91PTT/9PEN, and PEN, respectively. For each Figure, it shows the linear relationship between the observed T_m and T_c, within the T_c range studied. The intersection of a least square line, fit to the data set of each sample, with the line $T_m = T_c$ provides the values of T_m^o. The slope of the least square line, which equals 1/2β, can also be used to calculate β parameter (i.e., $\beta = 0.5 \times \text{slope}^{-1}$). The T_m^o, β, and χ^2 (suggesting the quality of the fit) values for each sample were summarized in Table 2. The value of β near one guaranteed (base on the assumptions of the Hoffman-Weeks derivation) that the extrapolation was valid and gave a reliable T_m^o value, because the T_m values observed for different T_c values were not greatly affected by the lamellar thickening process.

Although the non-linearity in the observed T_m-T_c data over a wide range of the temperature was explained to some extent by Alamo *et al.* [17], it is the recent contribution by Marand *et al.* [18] that offers a new extrapolative procedure to determine the T_m^o value of a semi-crystalline polymer based on the observed T_m-T_c data in which the observed T_m data were taken from samples crystallized at different temperatures but with the same a priori lamellar thickening coefficient. Derived based on the Gibbs-Thomson equation [19,20] and on the proposition of Lauritzen and Passaglia [21] on stem length fluctuation during chain folding, Marand *et al.* [18] proposed a new mathematical derivation which states a relationship between the observed melting temperature and the corresponding crystallization temperature. This equation is hereafter called the non-linear Hoffmann-Weeks extrapolation (NLHW), which was written in the form:

$$\frac{T_m^o}{T_m^o - T_c} = \beta^m \frac{\sigma_e^l}{\sigma_e^{GT}} \left[\frac{T_m^o}{T_m^o - T_c} + \frac{D_2 \Delta H_f^o}{2\sigma_e^l} \right] \quad , \tag{4}$$

or in a simpler form:

$$M = \beta^m \frac{\sigma_e^l}{\sigma_e^{GT}} (X + a) \quad , \tag{5}$$

where β^m is the thickening coefficient, σ_e^{GT} is the fold surface free energy associated with nuclei of critical size including the extra lateral surface energy due to fold protrusion and the mixing entropy associated with stems of different lengths (σ_e^{GT} is the basal interfacial energy as appeared in the Gibbs-Thomson equation), σ_e^l is the interfacial energy associated with the basal plane of the mature crystallite, D_2 is a constant, and all other parameters are the same as previously defined. It is worth nothing that, for most cases, it is safe to assume that $\sigma_e^l \approx \sigma_e^{GT}$ [18].

In order to apply Equation (5), the reduced parameters M and X have to be calculated from a set of the observed T_m-T_c data, such as those summarized in Table 1 for all of the sample investigated, based on an initial guess value of T_m^o. The true T_m^o value is the guessed T_m^o value which results in the slope of the M-X plot of 1 (i.e., $\beta^m = 1$). According to this procedure, the NLHW prediction is shown as solid line in Figure 4(a)-4(e) and the T_m^o, β^m, and χ^2 values for each sample were summarized in Table 2.

In addition, one can see that the melting point depression was found in the PTT-blends system. Generally, the melting point depression of semicrystalline polymer and its blend results from morphological, kinetics, and thermodynamic effects [4,11]. Thermodynamic dictates that the chemical potential of PTT is decrease by the presence of PEN component, resulting in the depression of melting point. The interaction between PTT and PEN may affect the T_m^o value. Imperfect crystals may be caused by addition of PEN so the T_m^o value decreases.

3.4 Overall Isothermal Melt-Crystallization Kinetics

Isothermal bulk crystallization kinetics of semicrystalline polymers in a DSC is usually studied by following the crystallization exotherms [22,23], based on

the assumption that the evolution of crystallinity is linearly proportional to the evolution of heat released during the course of crystallization. Based on this notion, the relative crystallinity as a function of time θ(t) can be obtained according to the following equation:

$$\theta(t) = \frac{\int_0^t \left(\frac{dH_c}{dt}\right) dt}{\int_0^\infty \left(\frac{dH_c}{dt}\right) dt} \in [0,1] \quad , \qquad (6)$$

where t and ∞ are the elapsed time during the course of crystallization and at the end of crystallization process, respectively, and dH_c is the enthalpy of crystallization released during and infinitesimal time interval dt.

Figure 5(a)-5(e) illustrate the time-dependent relative crystallinity function θ(t) (after subtraction of the induction time t_0), which crystallized different crystallization temperatures T_c for PTT, 97PTT/3PEN, 94PTT/6PEN, 91PTT/9PEN, and PEN, respectively. It should be noted that the raw data are shown in those Figures as different geometry points for each crystallization temperature. For all samples, they are clearly that the time to reach the ultimate crystallinity (i.e., complete crystallization) increased with increasing crystallization temperature T_c. For PTT-blends system considered at the same T_c, the time to reach the ultimate crystallinity of 97PTT/3PEN was lower than that of pure PTT. As the content of PEN was further increased to 6 and 9 % wt, the time to reach the ultimate crystallinity dramatically increased. An important bulk or overall kinetic parameter which can be determined directly from the θ(t) data is the half-time of crystallization $t_{0.5}$, which is defined as the elapsed time measured from the onset of crystallization until the crystallization is half-completed. Table 3 summarizes the values of crystallization half-time $t_{0.5}$ taken from all of the experimental θ(t) data. According to Table3, it is apparent that the half-time of crystallization $t_{0.5}$ of all samples increase with increasing crystallization temperature T_c, at least within temperature range studied. For PTT-blends system considered at the same T_c, the half-time of crystallization $t_{0.5}$ of 97PTT/3PEN was lower than that of pure PTT. As the content of PEN was further increased to 6 and 9 % wt, the half-time of crystallization $t_{0.5}$ dramatically increased, as shown in Figure 6.

Figure 7 illustrates the plots between the half-time of crystallization $t_{0.5}$ and undercooling of PTT and the blends. It is evident that all of the polymers studied exhibited decreased crystallization half-time with increasing degree of undercooling (or with decreasing crystallization temperature). For the same undercooling, the half-time of crystallization $t_{0.5}$ decreased with increasing PEN content.

(a) Isothermal crystallization kinetics based on the Avrami analysis

Analysis of the time-dependent relative crystallinity function θ(t) is usually carried out in the context of the Avrami equation [24-29], which can be expressed as:

$$\theta(t) = 1 - \exp\left[-(K_a t)^{n_a}\right] \in [0,1] \quad , \tag{7}$$

where K_a and n_a are the Avrami crystallization rate constant and the Avrami exponent, respectively. Usually, the Avrami rate constant K_a is written in the form of the composite Avrami rate constant k_a (i.e., $k_a = K_a^n$). It was shown that k_a (the dimension of which is given in $(\text{time})^{-n}$) is not only a function of temperature, but also a function of the Avrami exponent n_a [30]. As a result, use of K_a should be more preferable than use of k_a due partly to the facts that it is independent of the Avrami exponent n_a and its dimension is given in $(\text{time})^{-1}$. It should be noted that both K_a and n_a are constants specific to a given crystalline morphology and type of nucleation for a particular crystallization condition [31] and that, based on the original assumptions of the theory, the value of the Avrami exponent n_a should be an integer ranging from 1 to 4.

Data analysis based on the Avrami kinetic equation is carried out by directly fitting the experimental θ(t) data obtained for each crystallization temperature to Equation (7) (shown in Figure 5 as solid lines). As a result, the Avrami kinetics parameters (i.e., n_a and K_a) along with χ^2 parameter were obtained. These parameters are summarized in Table 3. For all samples, the Avrami exponent n_a ranges from 2.03 to 2.86, which, according to the definition of the Avrami exponent [31], may correspond to a two dimensional growth with a combination of thermal and athermal nucleation (as a result of the fractional n_a values observed). More specifically, n_a ranges from 2.34 to 2.73 for PTT; from 2.40 to 2.86 for

97PTT/3PEN; from 2.11 to 2.69 for 94PTT/6PEN; from 2.60 to 2.78 for 91PTT/9PEN; and, lastly, from 2.03 to 2.48 for PEN.

According to Table 3, the rate of isothermal crystallization can readily be described by the values of the Avrami crystallization rate constant K_a and the crystallization half-time $t_{0.5}$ (or, more specifically the reciprocal value of the crystallization half-time $t_{0.5}^{-1}$). The result shows that, for each sample, the Avrami rate constant K_a and the reciprocal crystallization half-time $t_{0.5}^{-1}$ are found to decrease monotonically with increasing crystallization temperature T_c, suggesting that samples crystallize faster with decreasing T_c. For PTT-blends system considered at the same T_c, the Avrami rate constant K_a and the reciprocal crystallization half-time $t_{0.5}^{-1}$ of 97PTT/3PEN are greater than those of pure PTT. As the content of PEN was further increased to 6 and 9 % wt, the Avrami rate constant K_a and the reciprocal crystallization half-time $t_{0.5}^{-1}$ dramatically decreased, as shown in Figure 8 and 9, respectively.

Figure 10 and 11 illustrate, respectively, the Avrami rate constant K_a and the reciprocal crystallization half-time $t_{0.5}^{-1}$ versus degree of undercooling for PTT and the blends. It should be noted that such a plot of the reciprocal half-time of crystallization $t_{0.5}^{-1}$ versus degree of undercooling is regarded as the most fundamental representation of the bulk crystallization rate of a semi-crystalline polymer. Those figures are evident that all of the polymers studied exhibited increased the Avrami rate constant and the reciprocal crystallization half-time with increasing degree of undercooling (or with decreasing crystallization temperature). Considering a same degree of undercooling, 91PTT/9PEN exhibited the highest value of K_a and $t_{0.5}^{-1}$ followed by that of 94PTT/6PEN, 97PTT/3PEN, and PTT, respectively. The results clearly indicated that 91PTT/9PEN crystallized the fastest, followed 94PTT/6PEN, 97PTT/3PEN, and PTT, respectively.

(b) Isothermal crystallization kinetics based on the Malkin analysis

Derived based on a postulation that the overall crystallization rate equals the summation of the rate at which the degree of crystallinity varies with the emergence

of the primary nuclei and the rate of variation in the degree of crystallinity varies with the crystal growth rate, Malkin *et al.* [32] arrived at totally different kinetic equation:

$$\theta(t) = 1 - \frac{C_0 + 1}{C_0 + \exp(C_1 t)} \in [0,1] \quad , \tag{8}$$

where C_0 is the Malkin exponent which relates directly to the ratio of the crystal growth rate G to the primary nucleation rate I (i.e., $C_0 \alpha$ G/I), and C_1 is the Malkin crystallization rate constant which relates directly to overall crystallization (i.e., C_1 = aG+bI, where a and b are some specific constants). It should be noted that the dimension of the Malkin rate constant is given in $(\text{time})^{-1}$.

Data analysis based on the Malkin kinetic equation is carried out by directly fitting the experimental $\theta(t)$ data obtained for each crystallization temperature to Equation (8) (shown in Figure 5 as dash lines). Table 4 summarizes the Malkin kinetics parameters (i.e., C_0 and C_1) along with the χ^2 parameter obtained as a result of the best fit. According to Table 4, the Malkin exponent C_0 ranges from 23.38 to 49.22 for PTT; from 27.87 to 62.20 for 97PTT/3PEN; from 15.44 to 43.68 for 94PTT/6PEN; from 31.26 to 55.01 for 91PTT/9PEN; and, lastly, from 13.65 to 32.52 for PEN. For the Malkin crystallization rate constant C_1, it apparently exhibits a similar trend to that suggested by the reciprocal crystallization half-time $t_{0.5}^{-1}$ and the Avrami rate constant K_a in that it decreases with increasing crystallization temperature T_c for all samples studied. Moreover, for PTT-blends system considered at the same T_c and considered at the same undercooling ΔT, the C_1 values are also similar behavior to the Avrami rate constant K_a, as shown in Figure 12 and 13, respectively.

(c) Isothermal crystallization kinetics based on the Urbanovici-Segal analysis

Recently, Urbanovici and Segal [33] proposed a new macrokinetic equation, which is essentially a generalization of the Avrami model. In this proposition, the relation between the relative crystallinity as a function of time $\theta(t)$ and the crystallization time t is written as:

$$\theta(t) = 1 - \left[1 + (r-1)(K_{us}t)^{n_{us}}\right]^{1/(1-r)} \in [0,1] \quad , \qquad (9)$$

where K_{us} and n_{us} are the Urbanovici-Segal crystallization rate constant and the Urbanovici-Segal exponent, respectively. r is the parameter which satisfies the condition $r > 0$. At the condition where $r \rightarrow 1$, the Urbanovici-Segal model becomes identical to the Avrami model [33]. This may simply means that parameter r is merely the factor determining the degree of deviation of the Urbanovici-Segal model from the Avrami model. It is also worth noting that the Urbanovici-Segal kinetics parameters (i.e., K_{us} and n_{us}) have similar physical meanings to the Avrami kinetic parameters (i.e., K_a and n_a), and that the dimension of K_{us} is also given in $(\text{time})^{-1}$.

Data analysis based on the Urbanovici-Segal kinetic equation is carried out by directly fitting the experiment $\theta(t)$ data obtained for each crystallization temperature to Equation (9) (shown in Figure 5 as dotted lines). Table 5 summarizes the Urbanovici-Segal kinetics parameters (i.e., n_{us}, K_{us}, and r) along with the χ^2 parameter obtained as a result of the best fit. According to Table 5, the Urbanovici-Segal exponent n_{us} are found to range from 2.34 to 2.62 for PTT; from 2.22 to 2.98 for 97PTT/3PEN; from 2.16 to 2.92 for 94PTT/6PEN; from 2.33 to 2.86 for 91PTT/9PEN; and, lastly, from 2.13 to 2.41 for PEN. The Urbanovici-Segal rate constant K_{us} apparently exhibits a similar trend to that suggested by the other crystallization rate parameters in that it decreases with increasing crystallization temperature for all sample studied. For PTT-blends system considered at the same T_c and considered at the same undercooling ΔT, the K_{us} values are also similar trend like the other kinetics rate parameters (i.e., $t_{0.5}^{-1}$, K_a, C_1), as shown in Figure 14 and 15.

3.5 Isothermal Growth Rate

By measuring the spherulitic radius from PLM micrographs taken successive intervals during the isothermal crystallization, the growth rate was determine by a linear least squares fit of the initial linear portion of the growth rate curves before impingement. Figure 16(a)-16(d) give plots of the spherulitic radius versus time for different crystallization temperatures for PTT, 97PTT/3PEN, 94PTT/6PEN, and 91PTT/9PEN, respectively. The solid lines represent the best

least squares fit to the data. It is clear that there is a linear increase in the radius with time. The slope of the each straight line refers to the spherulitic growth rate of each crystallization temperatures. The spherulite growth rates G for PTT, 97PTT/3PEN, 94PTT/6PEN, and 91PTT/9PEN were summarized in Table 6-9, respectively. The plots of growth rate G as a function of crystallization temperature T_c are displayed in Figure 17. In the range of crystallization studied, growth rate G of all samples decreased dramatically as the crystallization temperature T_c is increased. For PTT-blends system considered at the same T_c in ranging from 190 to 202.5°C, the growth rate of 97PTT/3PEN was greater than that of pure PTT. As the content of PEN was further increased to 6 and 9 % wt, the growth rate G dramatically decreased, as shown in Figure 18. Interestingly, the growth rate behavior is a similar to the other overall crystallization rate parameters (i.e., $t_{0.5}^{-1}$, K_a, C_1, K_{us} as shown in Figure 8, 9, 12, and 14, respectively).

Figure 19 shows the plots of growth rate versus degree of undercooling for PTT, 97PTT/3PEN, 94PTT/6PEN, and 91PTT/9PEN. For a same undercooling, the spherulite growth rate of 97PTT/3PEN is higher than that of pure PTT. For the blends with PEN content ranging from 3 to 9 % wt, the data points are interpolated by the same curve, indicating that, for a same undercooling, spherulite growth rates in the blends are unaffected by composition in range studied.

In the context of the Lauritzen-Hoffman secondary nucleation theory [19], the linear growth rate G of a crystalline aggregate (e.g., spherulite or axialite) for each regime is dependent on the degree of undercooling ΔT, and is defined by the following equation:

$$G = G_0 \exp\left[-\frac{U^*}{R(T_c - T_\infty)}\right]\exp\left[-\frac{K_g}{T_c(\Delta T)f}\right] \qquad (10)$$

where G_0 is a pre-exponential term which is not strongly dependent on temperature. The first exponential term in Equation (10) contains the contribution of diffusion process to the growth rate, where U^* is the activation energy for the transportation of segments of molecules across the melt/solid surface boundary and is usually given by a universal value of 1500 cal mol^{-1}, T_c is the crystallization temperature, T_∞ is the temperature where the molecular motion ceases (i.e., $T_\infty = T_g - 30$), R is the

universal gas constant. The second exponential term relates to the formation of the critical nucleus on the growth face, where K_g is the nucleation exponent, ΔT is the degree of undercooling (i.e., $\Delta T = T_m^o - T_c$). The f factor is a correction coefficient for the temperature dependence of enthalpy of fusion, which is close to unity at high temperature (i.e., $f = 2T_c/(T_c + T_m^o)$).

For growth kinetic parameter analysis, it is convenient to rewrite Equation (10) as a logarithmic form as follows:

$$\log G + \frac{U^*}{2.303R(T_c - T_\infty)} = \log G_0 - \frac{K_g}{2.303T_c(\Delta T)f} \quad , \qquad (11)$$

In practice, the test of regimes can be done through the plot of the left-hand side of Equation (11) versus $1/2.303Tc(\Delta T)f$ (i.e., hereafter the LH plot). The slope of the plot equals $-K_g$. The G_0 of each regime can be calculated from the y-interception of each regime on the plot (i.e., $G_0 = 10^{(\text{y-intercept value})}$. According to Equation (11), regime I→II transition is evident when a downward change in slope is observed, whereas it is an upward change in slope that is observed in the transition from regime II to regime III [34]. Figure 20(a)-20(d) illustrate the LH plots of PTT, 97PTT/3PEN, 94PTT/6PEN, and 91PTT/9PEN, respectively. Both of PTT and 91PTT/9PEN showed the transition temperatures between regime III and II about 194°C while those of 97PTT/3PEN and 94PTT/6PEN could not observed from this crystallization temperature T_c range studied. However, the regime growth of 97PTT/3PEN and 94PTT/6PEN was found to be regime II for crystallization temperature range studied. The $K_{g(III)}/K_{g(II)}$ ratios of PTT and 91PTT/9PEN are 2.19 and 2.01, respectively, which is very close to 2.0 as predicted by the Lauritzen-Hoffman theory. The calculated K_g and G_0 values of all samples were listed in Table 10.

From general thermodynamic consideration, the factor K_g is very important because it contains the variable ξ reflecting the regime behavior. K_g is given by:

$$K_g = \frac{\xi b_0 \sigma \sigma_e T_m^o}{k \Delta h_f^o} \quad , \qquad (12)$$

where ξ equals 2 for regime II and 4 for regime I and III, b_0 is the crystal layer thickness, σ and σ_e are the lateral and fold surface free energy, respectively, T_m^o is the equilibrium melting temperature, k is the Boltzmann's constant, and Δh_f^o is the equilibrium heat of fusion per unit volume (i.e., $\Delta h_f^o = \Delta H_f^o x \rho_c$). To calculate $\sigma\sigma_e$, for PTT, the input parameters are the layer thickness b_0 = 5.71 Å (the (010) crystal plane) [35], the equilibrium heat of fusion ΔH_f^o = 145.6 J g^{-1} [36], the crystallographic density ρ_c = 1.40 g cm^{-3} [37], and the equilibrium melting temperatures T_m^o listed in Table 2. According to Equation (12), the $\sigma\sigma_e$ values can be calculated.

The lateral surface free energy σ may be estimate based on the modified Thomas-Staveley equation [38]:

$$\sigma = \alpha \Delta h_f^o \sqrt{a_0 b_0} \quad , \tag{13}$$

where a_0 and b_0 is the molecular width (4.63 Å for PTT) [37] and molecular layer thickness (5.71 Å for PTT) [35], respectively. Generally, the Thomas-Staveley constant α is usually assumed to be $\approx$ 0.1. However, the α value is not at all universal and strongly dependent on the chemical structure of polymer. For PTT, the α value, calculated by Hong *et al.* [35], equals 1.8. According to Equation (13), the lateral surface free energy σ can be calculated to be 18.87 erg cm^{-2}. At this point, σ_e can be calculated from $\sigma\sigma_e$.

The average work of chain folding $\bar{q}$ has been found to be one parameter most closely correlated with molecular structure, and probably the most important contribution to its relative magnitude is thought to be the inherent stiffness of the chain itself [39]. The average work of chain folding $\bar{q}$ which is defined as:

$$\bar{q} = 2 a_0 b_0 \sigma_e \quad , \tag{14}$$

can be also calculated. The values of K_g, $\sigma\sigma_e$, σ_e, and $\bar{q}$ were summarized in Table 10.

3.6 Morphology of crystallite

Figure 21, 22, 23, and 24, respectively, illustrate series of PLM micrographs for PTT, 97PTT/3PEN, 94PTT/6PEN, and 91PTT/9PEN isothermally crystallized at various crystallization temperature T_c. In general, PTT bulk polymer forms spherulites when it is crystallized from the melt. These spherulites revealed a dark Maltese cross along the vibrational directions of polarizer and analyzer. When PTT was crystallized at T_c lower than 202.5°C banding can be found in the spherulites. Banded spherulites of PTT/PEN blends were observed at crystallization temperature ranging from 185 to 200°C for 97PTT/3PEN and 94PTT/6PEN; and, from 185 to 197.5°C for 91PTT/9PEN. The spacing of bands of PTT increases with increasing T_c, as shown in Figure 21. The formation of banded structure could be attributed to the lamellar twisting during growth [40]. The spherulite texture becomes finer as T_c is decreased.

Figure 25 shows a series of spherulites crystallized at 190°C in PTT containing various PEN content. The body of spherulite texture is more open with increasing PEN content. PEN, rejected species by growing crystal, diffuses to interfibrillar regions, where increases in its concentration have the effect of retarding further crystallization when considering at the same T_c. More open textures can be observed by working at small undercooling so as to cause molecules to be more rejected to some extent, then spherulite are very coarse and irregular in shape, as shown in Figure 26. Change in the boundary of spherulite with composition was also observed in Figure 27.

4. CONCLUSIONS

In this study, the miscibility, melting, crystallization behaviors, and morphologies of PTT blends have been investigated. From DSC measurement, PTT/PEN blends are miscible in amorphous state for composition range studied based on single T_g of these blends. The T_g and T_{cc} (cold-crystallization temperature) rises monotonically with increasing PEN content in the blends. The relationship between T_g and composition in these blends can be fitted well by the Gordon-Taylor equation.

The subsequent melting endotherms for PTT/PEN blends exhibited either triple (at T_c lower than 195°C for PTT and 97PTT/3PEN; at T_c lower than 192.5 for

94PTT/6PEN and 91PTT/9PEN) or double melting phenomena (at T_c greater than 195°C for PTT and 97PTT/3PEN; at T_c greater than 192.5 for 94PTT/6PEN and 91PTT/9PEN). These peaks were denoted peaks I, II, and III for low-, middle-, and high-temperature melting endotherm, respectively. For triple melting phenomenon, it was postulated that the occurrence of peak I was a result of the melting of the primary crystallites, peak II was a result of the melting of recrystallized crystallites, and peak III was a result of the melting of the recrystallized crystallites of different stabilities. The endothermic peaks I of the blends, corresponded primary melting at a various T_c, was used to determine T_m^o. Both LHW and NLHW show that T_m^o decreases with increasing PEN content.

All of the overall crystallization rate parameters (i.e., $t_{0.5}^{-1}$, K_a, C_1, and K_{us}) were found to be very sensitive to changes in the crystallization temperature. Within the crystallization temperature range studied (i.e., $190 \leq T_c \leq 205$ °C), the values of the rate parameters for these blends were all found to increase with decreasing crystallization temperature (or with increasing degree of undercooling), suggesting that these blends crystallized at low temperatures faster than that at high temperatures. Considering at the same T_c, the $t_{0.5}^{-1}$, K_a, C_1, and K_{us} values of 97PTT/3PEN are greater than those of pure PTT. As the content of PEN was further increased to 6 and 9 % wt, these values dramatically decreased. In addition, considering a same degree of undercooling, 91PTT/9PEN exhibited the highest values of the $t_{0.5}^{-1}$, K_a, C_1, and K_{us} followed by that of 94PTT/6PEN, 97PTT/3PEN, and PTT, respectively. The results clearly that 91PTT/9PEN crystallized the fastest, followed 94PTT/6PEN, 97PTT/3PEN, and PTT, respectively.

From PLM measurement, linear growth rate of PTT/PEN blends were measured in the temperature range 185-210°C for melt-press film. The spherulite growth rate G of PTT/PEN blends decreased dramatically as the crystallization temperature T_c is increased. When PTT/PEN blends were considered at the same T_c in ranging from 190 to 202.5°C, the growth rate of 97PTT/3PEN was greater than that of pure PTT. As the content of PEN was further increased to 6 and 9 % wt, the growth rate G dramatically decreased. For a same undercooling, the spherulite growth rate of 97PTT/3PEN is higher than that of pure PTT. For the blends with

PEN content ranging from 3 to 9 % wt, the data points are interpolated by the same curve, indicating that, for a same undercooling, spherulite growth rates in the blends are unaffected by composition in range studied. Using $U^* = 1500$ cal mol^{-1} together with determine T_g and T_m^o, the kinetic parameters G_o, K_g, σ, σ_e, $\bar{q}$ was determined. PTT and 91PTT/9PEN showed the transition temperatures between regime III and II about 194°C while those of 97PTT/3PEN and 94PTT/6PEN could not observed from this crystallization temperature T_c range studied. However, the regime growth of 97PTT/3PEN and 94PTT/6PEN was found to be regime II for crystallization temperature range studied.

Banded spherulites of PTT/PEN blends were observed at crystallization temperature ranging from 185 to 202.5°C for PTT; from 185 to 200°C for 97PTT/3PEN and 94PTT/6PEN; from 185 to 197.5°C for 91PTT/9PEN. The spacing of bands of PTT increases with increasing T_c. The spherulite texture becomes finer as T_c is decreased. The body of spherulite texture is more open with increasing PEN content. In addition, the boundary of spherulite is also changed with composition.

ACKNOWLEDGEMENTS

The authors wish to thank Dr. Hoe Chuah and his colleagues of Shell Chemical Company (USA) Ltd. for supplying PTT resin and for their kind assistance with molecular weight measurements. BP Chemical Company (USA) Ltd. for supplying PEN resin. Partial supports for this work from the Petroleum and Petrochemical Technology Consortium (through a governmental loan from the Asian Development Bank) and the Petroleum and Petrochemical College are gratefully acknowledged.

REFERENCES

[1] Whinfield, J. R.; Dickson, J. T. Brit Pat 578,079 (14 June 1946).

[2] *Process Economics Program Report 227. 1,3-Propanediol and Polytrimethylene Terephthalate*. SRI International (1999).

[3] Ward, I. M.; Wilding, M. A. *J. Polym. Sci., Polym. Phys. Ed.* 1976, 14, 263.

[4] Avramova, N. *Polymer* 1995, 36, 801.

[5] Saheb, D. N.; Jog, J. P. *J. Polym. Sci., Part B: Polym. Phys.* 1999, 37, 2439.

[6] Shi, Y.; Jabarin, S. A. *J. Appl. Polym. Sci.* 2001, 81, 23.

[7] Supaphol, P.; Dangseeyun, N.; Thanomkiat, P. Nithitanakul, M. *J. Polym. Sci., Part B: Polym. Phys.* 2004, 42, 676.

[8] Supaphol, P.; Dangseeyun, N.; Srimoaon, P. *Polymer Testing* 2004, 23, 175.

[9] Dangseeyun, N.; Supaphol, P.; Nithitanakul, M. *Polymer Testing* 2004, 23, 187.

[10] Huang, J. M.; Chang, F. C. *J. Appl. Polym. Sci.* 2002, 84, 850.

[11] Wu, P. L.; Woo, E. M. *J. Polym. Sci., Part B: Polym. Phys.* 2002, 40, 1571.

[12] Fox, T. G. *Bull. Am. Phys. Soc.* 1956, 2, 123.

[13] Gordon, M.; Taylor, J.S.; *J. Appl. Chem.* 1952, 2, 493.

[14] Srimoaon, P.; Dangseeyun, N.; Supaphol, P. *Euro. Polym. J.* 2004, 40, 599.

[15] Lee, W. D.; Yoo, E. S.; Im, S. S. *Polymer* 2003, 44, 6617.

[16] Hoffman, J. D.; Weeks, J. J. *J. Res. Natl. Bur. Stand.* 1962, A66, 13.

[17] Alamo, R. G.; Viers, B. D.; Mandelkern, L. *Macromolecules* 1995, 28, 3205.

[18] Marand, H.; Xu, J.; Srinivas, S. *Macromolecules* 1998, 31, 8219.

[19] Hoffman, J. D.; Davis, G. T.; Lauritzen, J. J. in: N. B. Hannay (Ed.), *"Treatise on Solid State Chemistry*, Vol. 3, Plenum Press, NewYork, 1976, Chapter 7.

[20] Brown, R. G.; Eby, R. K. *J. Appl. Phys.* 1964, 35, 1156.

[21] Lauritzen, J. J.; Passaglia, E. *J. Res. Natl. Bur. Stand.* 1967, A71, 261.

[22] Hay, J. N.; Sabir, M. *Polymer* 1969, 10, 203.

[23] Hay, J. N. *Brit. Polm. J.* 1979, 11, 137.

[24] Kolmogorov, A. N.; Izvestiya, Akad. USSR, Ser. Mater. 1, 1937, 355.

[25] Johnson, W. A.; Mehl, K. F. *Trans. Am. Inst. Mining. Met. Eng.* 1939, 135, 416.

[26] Avrami, M. *J. Chem. Phys.* 1939, 7, 1103.

[27] Avrami, M. *J. Chem. Phys.* 1940, 8, 212.

[28] Avrami, M. *J. Chem. Phys.* 1941, 9, 177.

[29] Evans, U.R. *Trans. Faraday Soc.* 1945, 41, 365.

[30] Supaphol, P.; Spruiell, J. E. *Polymer* 2001, 42, 699.

[31] Wunderlich, B. *Macromolecular Physics*, Vol. 2, Academic Press, New York, 1976, pp. 132-147.

[32] Malkin, A. Y.; Beghishev, V. P.; Keapin, I. A.; Bolgov, S. A. *Polym. Eng. Sci.* 1984, 24, 1396.

[33] Urbanovici, E.; Segal, E. *Thermochim. Acta* 1990,171, 87.

[34] Supaphol, P.; Spruiell, J. E. *Polymer* 2000, 41, 1205.

[35] Hong, P. D.; Chung, W. T.; Hsu, C. F. *Polymer* 2002, 43, 3335.

[36] Pyda, M.; Boller, A.; Grebowicz, J.; Chuah, H.; Lebedev, V.; Wunderlich, B. *J. Polym. Sci. Polym. Phys. Ed.* 1998, 36, 2499.

[37] Wang, B.; Li, C. Y.; Hanzlicek, J.; Cheng, S. Z. D.; Geil, P. H.; Grebowicz, J.; Ho, R. M. *Polymer* 2001, 42, 7171.

[38] Thomas, D. G.; Staveley, L. A. K. *J. Chem. Soc.* 1952, 4569.

[39] Huang, J. M.; Chang, F. C. *J. Polym. Sci., Part B: Polym. Phys.* 2000, 38, 934.

[40] Ho, R. M.; Ke, K. Z.; Chen, M. *Macromolecules* 2000, 33, 7529.

CAPTIONS OF FIGURES

Figure 1. DSC cold crystallization and melting thermograms for quenched PTT, PEN, and PTT/PEN blend samples recorded during heating at $10^{o}Cmin^{-1}$.

Figure 2. Observed glass transition temperature Tg for quenched PTT, PEN, and PTT/PEN blend samples as a function of blends composition.

Figure 3. Subsequent melting endotherms (recorded with a heating rate $10^{o}C\ min^{-1}$) for PTT, PEN, PTT/PEN blend samples isothermallly crystallized from melt-state at different crystallization temperatures.

Figure 4. Observed melting temperature of primary crystallites as a function of crystallization temperature for PTT, PEN, PTT/PEN blend samples.

Figure 5. Relative crystallinity as a function of time of PTT, PEN, PTT/PEN blend samples at different crystallization temperatures. The experimental data, shown as various geometrical points, were fitted to the Avrami, Malkin, and Urbanovici-Segal macrokinetics models in which the best fits according to these models are shown as the solid, dashed, and dotted lines, respectively.

Figure 6. Crystallization half time $t_{0.5}$ of PTT, PTT/PEN blends samples at various crystallization temperature.

Figure 7. Crystallization half time $t_{0.5}$ of PTT, PTT/PEN blends samples as a function of degree of undercooling.

Figure 8. Avrami rate constant K_a of PTT, PTT/PEN blends samples at various crystallization temperature.

Figure 9. Reciprocal half-time $t_{0.5}^{-1}$ of PTT, PTT/PEN blends samples at various crystallization temperature.

Figure 10. Avrami rate constant K_a of PTT, PTT/PEN blends samples as a function of degree of undercooling.

Figure 11. Reciprocal half-time $t_{0.5}^{-1}$ of PTT, PTT/PEN blends samples as a function of degree of undercooling.

Figure 12. Malkin rate constant C_1 of PTT, PTT/PEN blends samples at various crystallization temperatures.

Figure 13. Malkin rate constant C_1 of PTT, PTT/PEN blends samples as a function of degree of undercooling.

Figure 14. Urbanovici-Segal rate constant K_{us} of PTT, PTT/PEN blends samples at various crystallization temperatures.

Figure 15. Urbanovici-Segal rate constant K_{us} of PTT, PTT/PEN blends samples as a function of degree of undercooling.

Figure 16. Radius of spherulite as a function of time for PTT, PTT/PEN blends at different crystallization temperatures.

Figure 17. Spherulite growth rate of PTT, PTT/PEN blends samples as a function of crystallization temperatures.

Figure 18. Spherulite growth rate G of PTT, PTT/PEN blends samples at various crystallization temperatures.

Figure 19. Spherulite growth rate G of PTT, PTT/PEN blends samples as a function of degree of undercooling.

Figure 20. Analysis of the spherulite growth rates of PTT, PTT/PEN blend samples as a function of crystallization temperature based on the Lauritzen and Hoffman secondary nucleation theory for the case $U^* = 1500$ cal mol^{-1}, $T_\infty (K) = T_g - 30$.

Figure 21. PLM micrographs of PTT spherulites crystallized at different crystallization temperatures.

Figure 22. PLM micrographs of 97PTT/3PEN spherulites crystallized at different crystallization temperatures.

Figure 23. PLM micrographs of 94PTT/6PEN spherulites crystallized at different crystallization temperatures.

Figure 24. PLM micrographs of 91PTT/9PEN spherulites crystallized at different crystallization temperatures.

Figure 25. Spherulite grown at 190°C in PTT, PTT/PEN blend samples.

Figure 26. Spherulite grown at 210°C in PTT, PTT/PEN blend samples.

Figure 27. Spherulite grown at 200°C in PTT, PTT/PEN blend samples.

Table 1.

Variation of low-melting peak temperature T_I for neat PTT and the blends, middle-melting peak temperature T_M for neat PEN and their enthalpies of fusion ΔH_f measured at various crystallization temperatures T_c

T_c	PTT		97PTT/3PEN		94PTT/6PEN		91PTT/9PEN		PEN	
(°C)	T_I (°C)	ΔH_f (J g^{-1})	T_I (°C)	ΔH_f (J g^{-1})	T_I (°C)	ΔH_f (J g^{-1})	T_I (°C)	ΔH_f (J g^{-1})	T_M (°C)	ΔH_f (J g^{-1})
190.0	210.683	1.362	209.183	2.208	208.850	2.620	208.683	3.255	-	-
192.5	212.341	3.121	210.675	3.856	210.508	4.528	210.175	4.452	-	-
195.0	213.866	4.887	212.533	6.288	212.533	4.840	211.633	7.426	-	-
197.5	215.858	7.075	214.025	9.768	213.858	10.983	213.125	8.538	-	-
200.0	217.350	10.119	215.850	11.663	215.350	12.700	214.650	11.224	-	-
202.5	218.841	11.434	217.175	12.923	216.675	12.433	216.175	13.231	-	-
205.0	220.200	9.795	218.700	10.852	218.033	12.920	217.700	12.639	-	-
237.5	-	-	-	-	-	-	-	-	259.191	12.137
240.0	-	-	-	-	-	-	-	-	260.850	11.836
242.5	-	-	-	-	-	-	-	-	262.508	16.048
245.0	-	-	-	-	-	-	-	-	264.200	21.961
247.5	-	-	-	-	-	-	-	-	265.725	24.407
250.0	-	-	-	-	-	-	-	-	267.016	44.197

Table 2.

Estimated equilibrium melting temperatures for PTT, 97PTT/3PEN, 94PTT/6PEN, 91PTT/9PEN, and PEN according to linear and non-linear Hoffman-Weeks extrapolations, along with other fitting parameters

Polymer	T_c range studied	LHW			NLHW		
	(°C)	T_m^o (°C)	β	χ^2	T_m^o (°C)	β^m	χ^2
PTT	190-205	248.227	0.777	0.99775	287.666	1.000	0.99677
97PTT/3PEN	190-205	243.513	0.780	0.99855	279.316	1.000	0.99781
94PTT/6PEN	190-205	239.004	0.820	0.99500	269.656	1.000	0.99345
91PTT/9PEN	190-205	236.753	0.832	0.99993	266.790	1.000	0.99995
PEN	237.5-250	296.969	0.789	0.99806	338.302	1.000	0.99715

Table 3.

Summary of the half-time of crystallization $t_{0.5}$, the reciprocal half-time $t_{0.5}^{-1}$, the Avrami kinetics parameters (i.e., n_a and K_a), and the χ^2 parameter suggesting the quality of the plots for PTT, 97PTT/3PEN, 94PTT/6PEN, 91PTT/9PEN, and PEN

	PTT					97PTT/3PEN					94PTT/6PEN					91PTT/9PEN					PEN				
T_c	$t_{0.5}$	$t_{0.5}^{-1}$	n_a	K_a	χ^2	$t_{0.5}$	$t_{0.5}^{-1}$	n_a	K_a	χ^2	$t_{0.5}$	$t_{0.5}^{-1}$	n_a	K_a	χ^2	$t_{0.5}$	$t_{0.5}^{-1}$	n_a	K_a	χ^2	$t_{0.5}$	$t_{0.5}^{-1}$	n_a	K_a	χ^2
(°C)	(min)	(min^{-1})		(min^{-1})		(min)	(min^{-1})		(min^{-1})		(min)	(min^{-1})		(min^{-1})		(min)	(min^{-1})		(min^{-1})		(min)	(min^{-1})		(min^{-1})	
190.0	1.491	0.670	2.45	0.574	0.99988	1.238	0.808	2.69	0.703	0.99977	1.520	0.658	2.61	0.570	0.99992	2.057	0.486	2.75	0.424	0.99996	-	-	-	-	-
192.5	2.206	0.453	2.34	0.385	0.99979	1.547	0.646	2.77	0.565	0.99996	1.902	0.526	2.54	0.452	0.99977	2.555	0.391	2.67	0.341	1.00000	-	-	-	-	-
195.0	2.720	0.368	2.44	0.315	0.99995	2.033	0.492	2.85	0.431	0.99993	2.809	0.356	2.69	0.309	0.99985	3.828	0.261	2.72	0.228	0.99999	-	-	-	-	-
197.5	4.195	0.238	2.38	0.204	0.99998	3.041	0.329	2.79	0.287	0.99995	4.067	0.246	2.63	0.212	0.99979	4.669	0.214	2.60	0.186	0.99999	-	-	-	-	-
200.0	5.480	0.182	2.42	0.157	0.99993	4.114	0.243	2.86	0.214	0.99999	5.514	0.181	2.61	0.157	0.99996	6.949	0.144	2.73	0.126	0.99998	-	-	-	-	-
202.5	8.485	0.118	2.65	0.103	0.99991	6.631	0.151	2.57	0.130	0.99998	9.433	0.106	2.11	0.088	0.99991	10.019	0.100	2.47	0.086	0.99991	-	-	-	-	-
205.0	14.121	0.071	2.73	0.062	0.99956	9.435	0.106	2.40	0.092	0.99978	14.192	0.070	2.55	0.061	0.99993	17.654	0.057	2.78	0.050	0.99989	-	-	-	-	-
237.5	-	-	-	-	-	-	-	-	-	-	-	-	-	-	-	-	-	-	-	-	1.397	0.716	2.24	0.608	0.99999
240.0	-	-	-	-	-	-	-	-	-	-	-	-	-	-	-	-	-	-	-	-	1.511	0.662	2.03	0.547	0.99959
242.5	-	-	-	-	-	-	-	-	-	-	-	-	-	-	-	-	-	-	-	-	2.215	0.452	2.13	0.380	0.99999
245.0	-	-	-	-	-	-	-	-	-	-	-	-	-	-	-	-	-	-	-	-	4.876	0.205	2.41	0.177	0.99989
247.5	-	-	-	-	-	-	-	-	-	-	-	-	-	-	-	-	-	-	-	-	6.881	0.145	2.48	0.126	0.99998
250.0	-	-	-	-	-	-	-	-	-	-	-	-	-	-	-	-	-	-	-	-	8.431	0.119	2.48	0.103	0.99968

Table 4.

Summary of the Malkin kinetics parameters (i.e., C_0 and C_1), and the χ^2 parameter suggesting the quality of the plots for PTT, 97PTT/3PEN, 94PTT/6PEN, 91PTT/9PEN, and PEN

	PTT			97PTT/3PEN			94PTT/6PEN			91PTT/9PEN			PEN		
T_c (°C)	C_0	C_1 (min^{-1})	χ^2	C_0	C_1 (min^{-1})	χ^2	C_0	C_1 (min^{-1})	χ^2	C_0	C_1 (min^{-1})	χ^2	C_0	C_1 (min^{-1})	χ^2
190.0	28.31	2.267	0.99970	42.27	3.052	0.99987	39.43	2.434	0.99977	51.22	1.922	0.99978	-	-	-
192.5	23.38	1.450	0.99954	54.08	2.590	0.99979	31.86	1.837	0.99969	46.09	1.511	0.99978	-	-	-
195.0	29.60	1.259	0.99970	60.30	2.024	0.99980	43.68	1.350	0.99973	49.05	1.023	0.99973	-	-	-
197.5	26.33	0.791	0.99967	56.10	1.328	0.99973	39.05	0.905	0.99968	39.90	0.797	0.99974	-	-	-
200.0	29.50	0.627	0.99956	62.20	1.009	0.99964	40.11	0.674	0.99967	50.02	0.567	0.99965	-	-	-
202.5	42.90	0.448	0.99956	37.43	0.551	0.99975	15.44	0.299	0.99938	31.26	0.349	0.99961	-	-	-
205.0	49.22	0.279	0.99902	27.87	0.360	0.99950	36.63	0.257	0.99951	55.01	0.229	0.99938	-	-	-
237.5	-	-	-	-	-	-	-	-	-	-	-	-	20.27	2.207	0.99961
240.0	-	-	-	-	-	-	-	-	-	-	-	-	13.65	1.786	0.99904
242.5	-	-	-	-	-	-	-	-	-	-	-	-	16.57	1.307	0.99960
245.0	-	-	-	-	-	-	-	-	-	-	-	-	28.26	0.698	0.99954
247.5	-	-	-	-	-	-	-	-	-	-	-	-	32.26	0.512	0.99964
250.0	-	-	-	-	-	-	-	-	-	-	-	-	32.52	0.421	0.99930

Table 5.

Summary of the reciprocal half-time $t_{0.5}^{-1}$, the Urbanovici-Segal kinetics parameters (i.e., n_{us}, K_{us}, and r), and the χ^2 parameter suggesting the quality of the plots for PTT, 97PTT/3PEN, 94PTT/6PEN, 91PTT/9PEN, and PEN

	PTT					97PTT/3PEN					94PTT/6PEN					91PTT/9PEN					PEN				
T_c (°C)	$t_{0.5}^{-1}$ (min^{-1})	n_{us}	K_{us} (min^{-1})	r	χ^2	$t_{0.5}^{-1}$ (min^{-1})	n_{us}	K_{us} (min^{-1})	r	χ^2	$t_{0.5}^{-1}$ (min^{-1})	n_{us}	K_{us} (min^{-1})	r	χ^2	$t_{0.5}^{-1}$ (min^{-1})	n_{us}	K_{us} (min^{-1})	r	χ^2	$t_{0.5}^{-1}$ (min^{-1})	n_{us}	K_{us} (min^{-1})	r	χ^2
190.0	0.670	2.62	0.595	1.151	1.00000	0.808	2.96	0.737	1.230	0.99992	0.658	2.76	0.586	1.125	1.00000	0.486	2.86	0.432	1.088	1.00000	-	-	-	-	-
192.5	0.453	2.58	0.404	1.201	0.99999	0.646	2.87	0.575	1.081	1.00000	0.526	2.81	0.475	1.226	1.00000	0.391	2.70	0.343	1.020	1.00000	-	-	-	-	-
195.0	0.368	2.55	0.322	1.089	1.00000	0.492	2.98	0.441	1.109	0.99999	0.356	2.92	0.321	1.180	1.00000	0.261	2.74	0.229	1.022	1.00000	-	-	-	-	-
197.5	0.238	2.42	0.206	1.040	0.99999	0.329	2.93	0.294	1.100	1.00000	0.246	2.89	0.222	1.206	1.00000	0.214	2.58	0.186	0.989	1.00000	-	-	-	-	-
200.0	0.182	2.34	0.154	0.913	0.99998	0.243	2.85	0.214	0.997	0.99999	0.181	2.69	0.159	1.065	0.99998	0.144	2.71	0.125	0.979	0.99999	-	-	-	-	-
202.5	0.118	2.53	0.100	0.893	0.99999	0.151	2.62	0.132	1.043	0.99999	0.106	2.16	0.090	1.048	0.99992	0.100	2.33	0.084	0.879	0.99999	-	-	-	-	-
205.0	0.071	2.51	0.059	0.779	0.99995	0.106	2.22	0.088	0.831	0.99999	0.070	2.46	0.060	0.917	0.99998	0.057	2.68	0.049	0.896	0.99996	-	-	-	-	-
237.5	-	-	-	-	-	-	-	-	-	-	-	-	-	-	-	-	-	-	-	-	0.716	2.21	0.604	0.977	0.99999
240.0	-	-	-	-	-	-	-	-	-	-	-	-	-	-	-	-	-	-	-	-	0.662	2.28	0.575	1.183	0.99989
242.5	-	-	-	-	-	-	-	-	-	-	-	-	-	-	-	-	-	-	-	-	0.452	2.13	0.380	1.006	0.99999
245.0	-	-	-	-	-	-	-	-	-	-	-	-	-	-	-	-	-	-	-	-	0.205	2.27	0.171	0.873	1.00000
247.5	-	-	-	-	-	-	-	-	-	-	-	-	-	-	-	-	-	-	-	-	0.145	2.41	0.124	0.945	1.00000
250.0	-	-	-	-	-	-	-	-	-	-	-	-	-	-	-	-	-	-	-	-	0.119	2.25	0.098	0.790	0.99999

Table 6.

Values of kinetics parameters calculated from the growth rate data of PTT ($U^* = 1500$ cal mol^{-1}, $T^o_{m(LHW)} = 248.227^oC$, $T_g = 39.206^oC$)

T_c (^oC)	T_c (K)	G (μm/sec)	log G (μm/sec)	log G + $U^*/2.303R(T_c-T_\infty)$	$f = 2T_c/(T^o_m+T_c)$	$1/2.303T_c(\Delta T)f$
185.00	458.15	0.8505	-0.0703	1.7943	0.9355	$1.602x10^{-5}$
187.50	460.65	0.6674	-0.1756	1.6629	0.9382	$1.655x10^{-5}$
190.00	463.15	0.4332	-0.3633	1.4497	0.9409	$1.711x10^{-5}$
192.50	465.65	0.3103	-0.5083	1.2801	0.9435	$1.773x10^{-5}$
195.00	468.15	0.2513	-0.5998	1.1645	0.9462	$1.842x10^{-5}$
197.50	470.65	0.2157	-0.6662	1.0746	0.9489	$1.917x10^{-5}$
200.00	473.15	0.1480	-0.8297	0.8884	0.9515	$2.000x10^{-5}$
202.50	475.65	0.1289	-0.8898	0.8060	0.9541	$2.092x10^{-5}$
205.00	478.15	0.1174	-0.9302	0.7439	0.9568	$2.196x10^{-5}$
207.50	480.65	0.0810	-1.0915	0.5616	0.9594	$2.312x10^{-5}$
210.00	483.15	0.0621	-1.2066	0.4259	0.9619	$2.444x10^{-5}$

Table 7.

Values of kinetics parameters calculated from the growth rate data of 97PTT/3PEN ($U^* = 1500$ cal mol^{-1}, $T^o_{m(LHW)} = 243.513^oC$, $T_g = 42.282^oC$)

T_c (^oC)	T_c (K)	G (μm/sec)	log G (μm/sec)	log G + $U^*/2.303R(T_c-T_\infty)$	$f = 2T_c/(T^o_m+T_c)$	$1/2.303T_c(\Delta T)f$
185.00	458.15	0.8341	-0.0788	1.8174	0.9401	$1.727x10^{-5}$
187.50	460.65	0.6630	-0.1785	1.6907	0.9428	$1.790x10^{-5}$
190.00	463.15	0.4819	-0.3170	1.5259	0.9455	$1.858x10^{-5}$
192.50	465.65	0.4396	-0.3569	1.4604	0.9482	$1.933x10^{-5}$
195.00	468.15	0.3397	-0.4689	1.3236	0.9509	$2.017x10^{-5}$
197.50	470.65	0.2660	-0.5752	1.1932	0.9535	$2.110x10^{-5}$
200.00	473.15	0.2084	-0.6812	1.0636	0.9562	$2.213x10^{-5}$
202.50	475.65	0.1508	-0.8215	0.9004	0.9588	$2.330x10^{-5}$
205.00	478.15	0.1158	-0.9364	0.7632	0.9614	$2.462x10^{-5}$
207.50	480.65	0.0663	-1.1783	0.4995	0.9640	$2.613x10^{-5}$
210.00	483.15	0.0498	-1.3026	0.3540	0.9666	$2.787x10^{-5}$

Table 8.

Values of kinetics parameters calculated from the growth rate data of 94PTT/6PEN ($U^* = 1500$ cal mol^{-1}, $T^{\circ}_{m(LHW)} = 239.004^{\circ}C$, $T_g = 45.536^{\circ}C$)

T_c ($^{\circ}C$)	T_c (K)	G (μm/sec)	log G (μm/sec)	$\log G + U^*/2.303R(T_c-T_\infty)$	$f = 2T_c/(T^{\circ}_m+T_c)$	$1/2.303T_c(\Delta T)f$
185.00	458.15	0.5743	-0.2408	1.6918	0.9445	$1.863x10^{-5}$
187.50	460.65	0.5287	-0.2768	1.6278	0.9472	$1.938x10^{-5}$
190.00	463.15	0.3826	-0.4172	1.4600	0.9499	$2.020x10^{-5}$
192.50	465.65	0.3133	-0.5040	1.3467	0.9526	$2.112x10^{-5}$
195.00	468.15	0.2603	-0.5846	1.2404	0.9553	$2.214x10^{-5}$
197.50	470.65	0.1812	-0.7418	1.0582	0.9579	$2.329x10^{-5}$
200.00	473.15	0.1488	-0.8273	0.9483	0.9606	$2.459x10^{-5}$
202.50	475.65	0.1134	-0.9456	0.8063	0.9632	$2.607x10^{-5}$
205.00	478.15	0.0748	-1.1261	0.6027	0.9658	$2.777x10^{-5}$
207.50	480.65	0.0446	-1.3510	0.3552	0.9684	$2.975x10^{-5}$
210.00	483.15	0.0334	-1.4762	0.2081	0.9710	$3.208x10^{-5}$

Table 9.

Values of kinetics parameters calculated from the growth rate data of 91PTT/9PEN ($U^* = 1500$ cal mol^{-1}, $T^o_{m(LHW)} = 236.753^oC$, $T_g = 46.134^oC$)

T_c (^oC)	T_c (K)	G (μm/sec)	log G (μm/sec)	$\log G + U^*/2.303R(T_c-T_\infty)$	$f = 2T_c/(T^o_m+T_c)$	$1/2.303T_c(\Delta T)f$
185.00	458.15	0.4871	-0.3124	1.6270	0.9467	$1.940x10^{-5}$
187.50	460.65	0.3772	-0.4235	1.4877	0.9494	$2.022x10^{-5}$
190.00	463.15	0.2954	-0.5296	1.3541	0.9521	$2.113x10^{-5}$
192.50	465.65	0.1989	-0.7013	1.1557	0.9548	$2.214x10^{-5}$
195.00	468.15	0.1463	-0.8348	0.9963	0.9575	$2.329x10^{-5}$
197.50	470.65	0.1216	-0.9152	0.8907	0.9601	$2.457x10^{-5}$
200.00	473.15	0.1094	-0.9610	0.8203	0.9628	$2.604x10^{-5}$
202.50	475.65	0.0804	-1.0945	0.6629	0.9654	$2.773x10^{-5}$
205.00	478.15	0.0570	-1.2440	0.4902	0.9680	$2.968x10^{-5}$
207.50	480.65	0.0319	-1.4962	0.2154	0.9706	$3.198x10^{-5}$
210.00	483.15	0.0243	-1.6136	0.0759	0.9732	$3.471x10^{-5}$

Table 10.

Input parameters and crystal growth parameters base on the traditional regime analysis for PTT, PTT/PEN blends ($U^* = 1500$ cal mol^{-1})

	PTT		97PTT/3PEN		94PTT/6PEN		91PTT/9PEN		Remarks
Input parameters									
T_m^o (K)	521.377		516.663		512.154		509.903		Data from Table 2
T_g (K)	312.356		315.432		318.686		319.284		Data from 3.1
Δh_f^o (erg cm^{-3})	2.038×10^9		2.038×10^9		2.038×10^9		2.038×10^9		Ref. [36], $\Delta h_f^o = \Delta H_f^o \times \rho_c$
Boltzmann's constant k (erg mol^{-1} K^{-1})	1.380×10^{-16}		1.380×10^{-16}		1.380×10^{-16}		1.380×10^{-16}		
Molecular width a_0 (cm)	4.63×10^{-8}		4.63×10^{-8}		4.63×10^{-8}		4.63×10^{-8}		Ref. [37]
Layer thickness b_0 (cm)	5.71×10^{-8}		5.71×10^{-8}		5.71×10^{-8}		5.71×10^{-8}		Ref. [35]
	Regime II	Regime III	Regime II	Regime III	Regime II	Regime III	Regime II	Regime III	
Kinetic parameters									
G_0 (μm sec^{-1})	2.88×10^3	14.79×10^5	12.88×10^3	-	5.62×10^3	-	0.96×10^3	0.83×10^5	
K_g (K^2)	1.25×10^5	2.74×10^5	1.37×10^5	-	1.13×10^5	-	0.84×10^5	1.70×10^5	
$\sigma\sigma_e$ (erg^2 cm^{-4})	590.56	647.25	653.15	-	543.48	-	405.78	410.61	
σ_e (erg cm^{-2})	31.30	34.30	34.61	-	28.80	-	21.50	21.76	
$\bar{q}$ (kcal mol^{-1})	2.38	2.6	2.63	-	2.19	-	1.63	1.65	

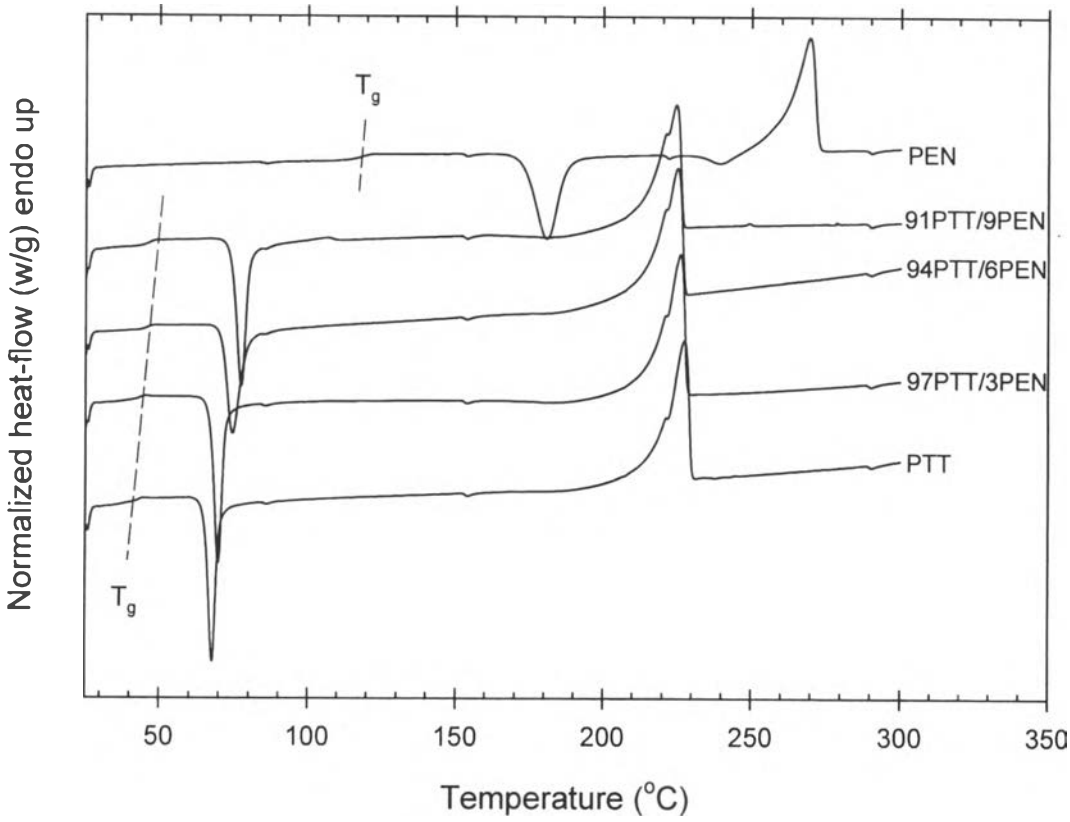
Normalized heat-flow (w/g) endo up
T_g
T_g
PEN
91PTT/9PEN
94PTT/6PEN
97PTT/3PEN
PTT
50
100
150
200
250
300
350
Temperature (°C)

Figure 1.

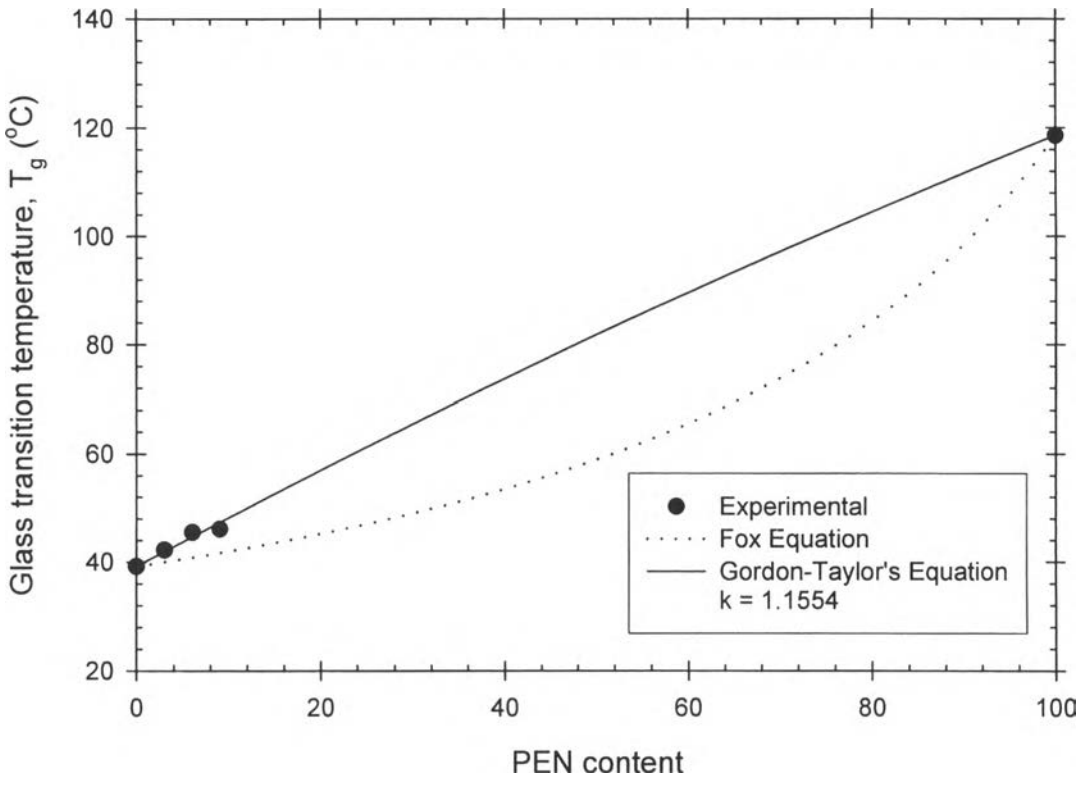
Glass transition temperature, T_g (°C)
PEN content
Experimental
Fox Equation
Gordon-Taylor's Equation
k = 1.1554
140
120
100
80
60
40
20
0
20
40
60
80
100

Figure 2.

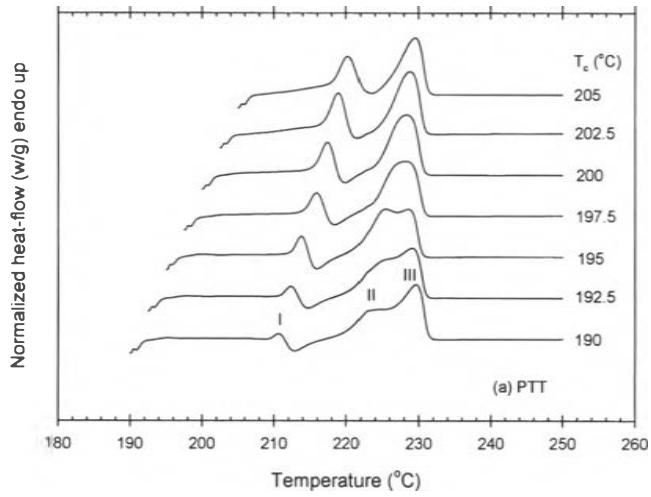
Normalized heat-flow (w/g) endo up
T_c (°C)
205
202.5
200
197.5
195
192.5
190
I
II
III
(a) PTT
180
190
200
210
220
230
240
250
260
Temperature (°C)

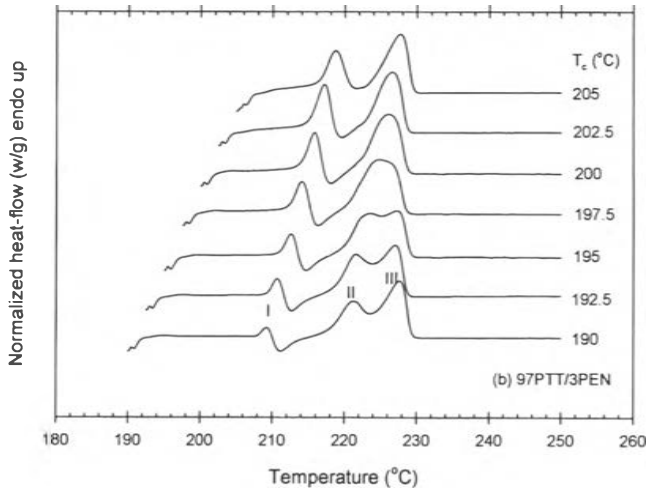
Normalized heat-flow (w/g) endo up
T_c (°C)
205
202.5
200
197.5
195
192.5
190
I
II
III
(b) 97PTT/3PEN
180
190
200
210
220
230
240
250
260
Temperature (°C)

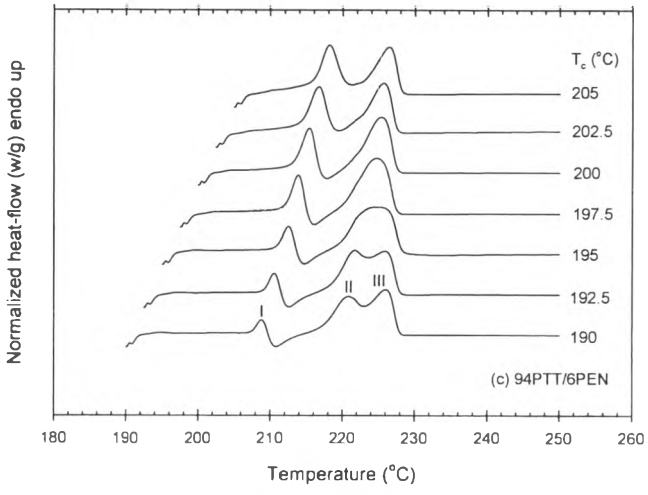
Normalized heat-flow (w/g) endo up
T_c (°C)
205
202.5
200
197.5
195
192.5
190
I
II
III
(c) 94PTT/6PEN
180
190
200
210
220
230
240
250
260
Temperature (°C)

Figure 3.

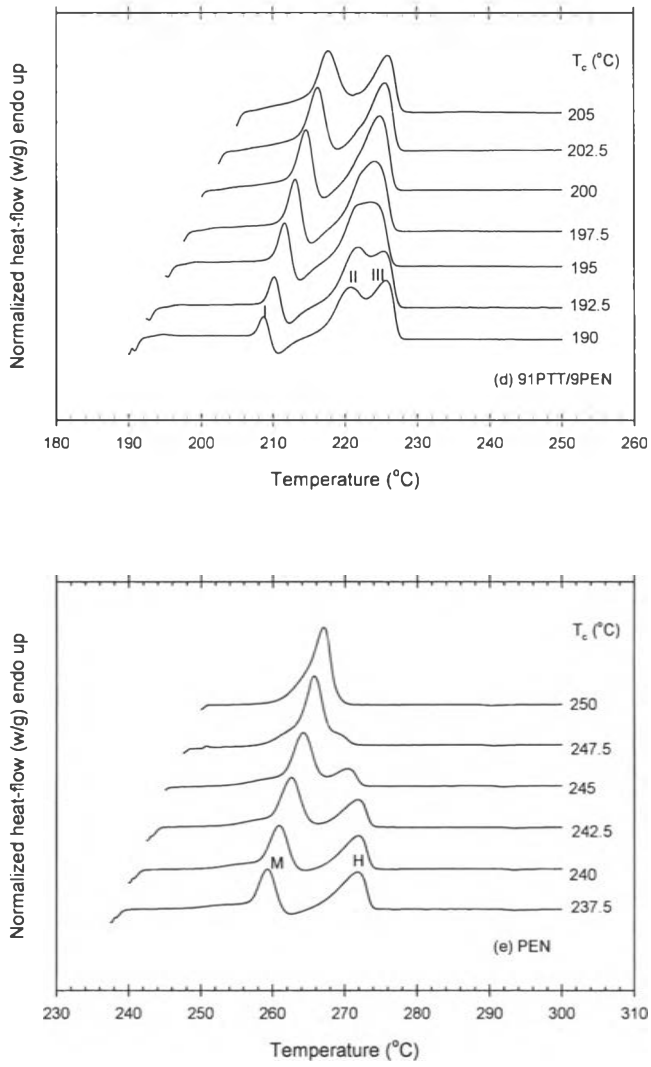

Figure 3. (continued)

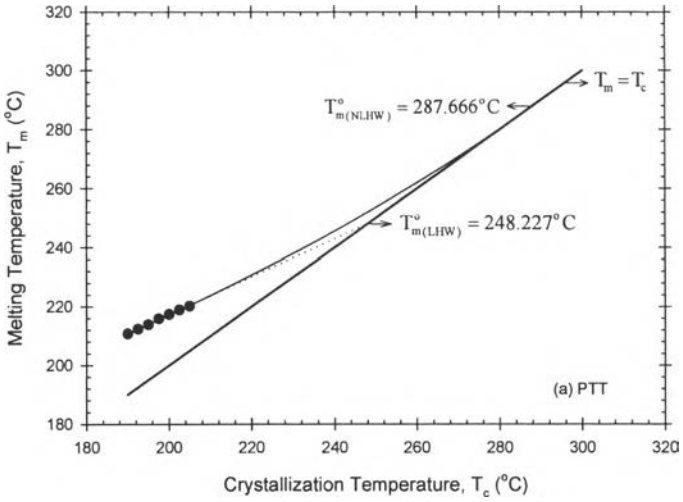
Melting Temperature, T_m (°C)
Crystallization Temperature, T_c (°C)
$T_m = T_c$
$T^o_{m(NLHW)} = 287.666°C$
$T^o_{m(LHW)} = 248.227°C$
(a) PTT

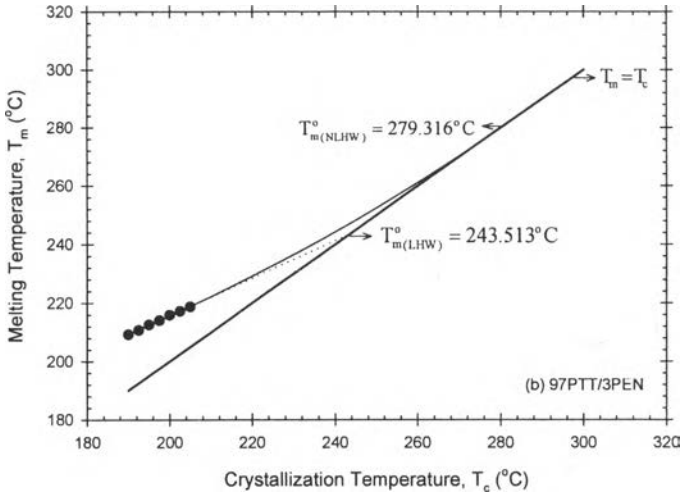
Melting Temperature, T_m (°C)
Crystallization Temperature, T_c (°C)
$T_m = T_c$
$T^o_{m(NLHW)} = 279.316°C$
$T^o_{m(LHW)} = 243.513°C$
(b) 97PTT/3PEN

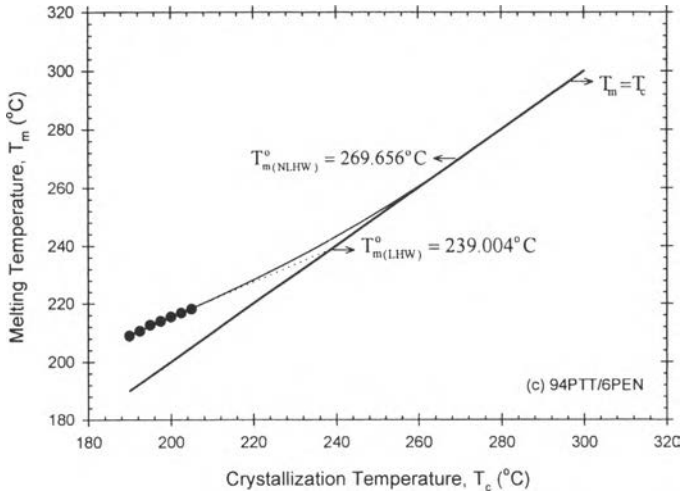
Melting Temperature, T_m (°C)
Crystallization Temperature, T_c (°C)
$T_m = T_c$
$T^o_{m(NLHW)} = 269.656°C$
$T^o_{m(LHW)} = 239.004°C$
(c) 94PTT/6PEN

Figure 4.

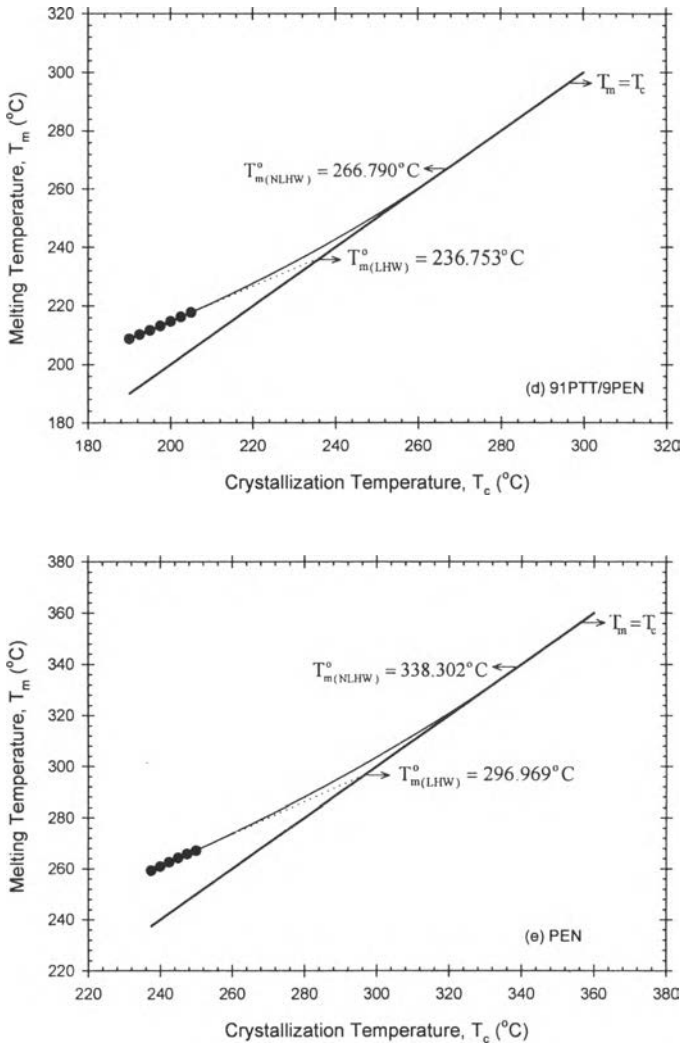

Figure 4. (continued)

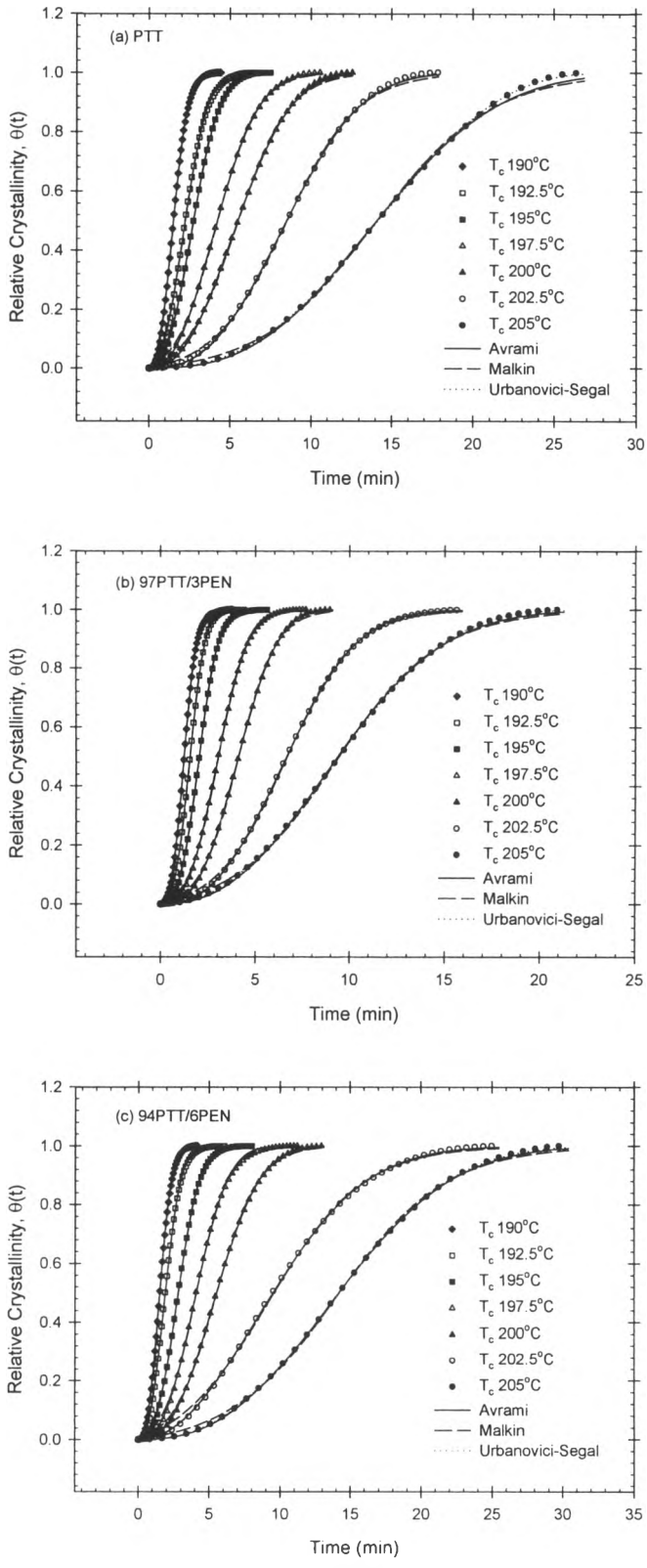
(a) PTT
(b) 97PTT/3PEN
(c) 94PTT/6PEN
Relative Crystallinity, θ(t)
Time (min)
T_c 190°C
T_c 192.5°C
T_c 195°C
T_c 197.5°C
T_c 200°C
T_c 202.5°C
T_c 205°C
Avrami
Malkin
Urbanovici-Segal

Figure 5.

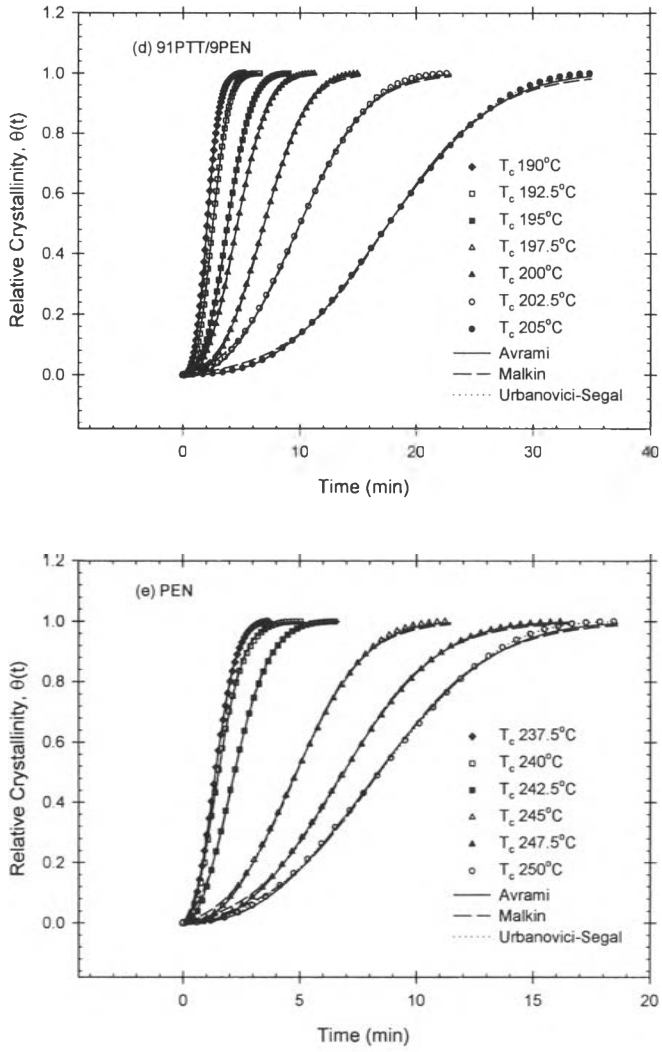

Figure 5. (continued)

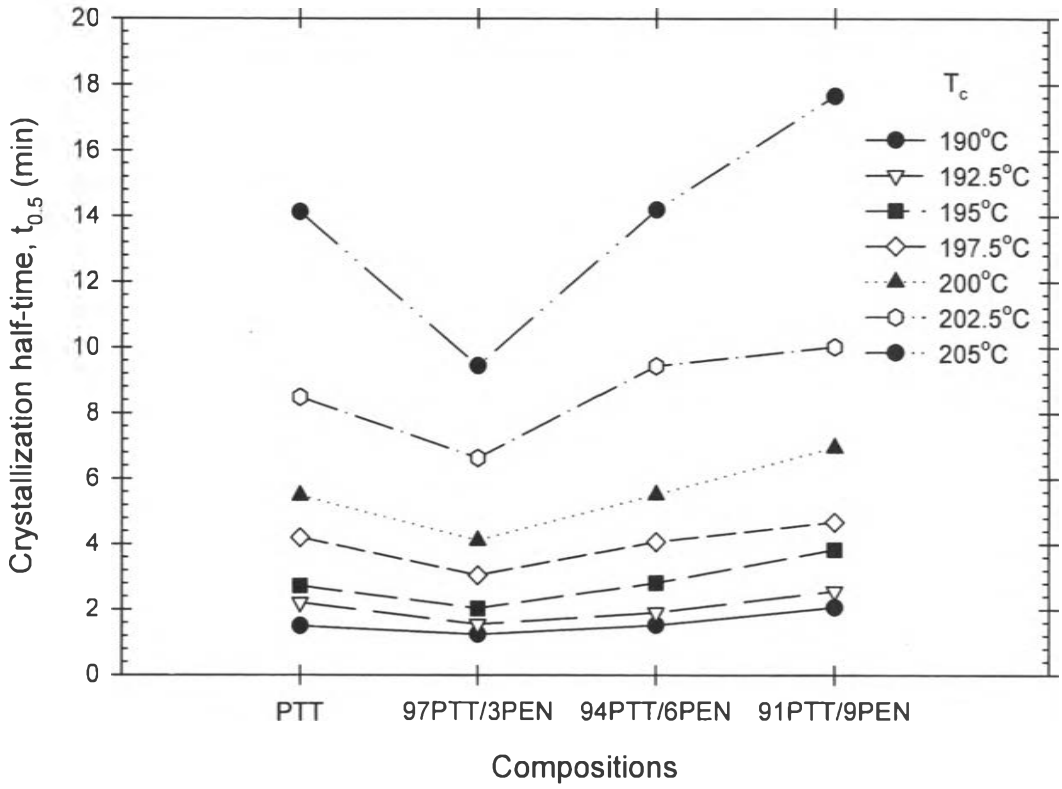
Crystallization half-time, $t_{0.5}$ (min)
20
18
16
14
12
10
8
6
4
2
0
PTT
97PTT/3PEN
94PTT/6PEN
91PTT/9PEN
Compositions
T_c
190°C
192.5°C
195°C
197.5°C
200°C
202.5°C
205°C

Figure 6.

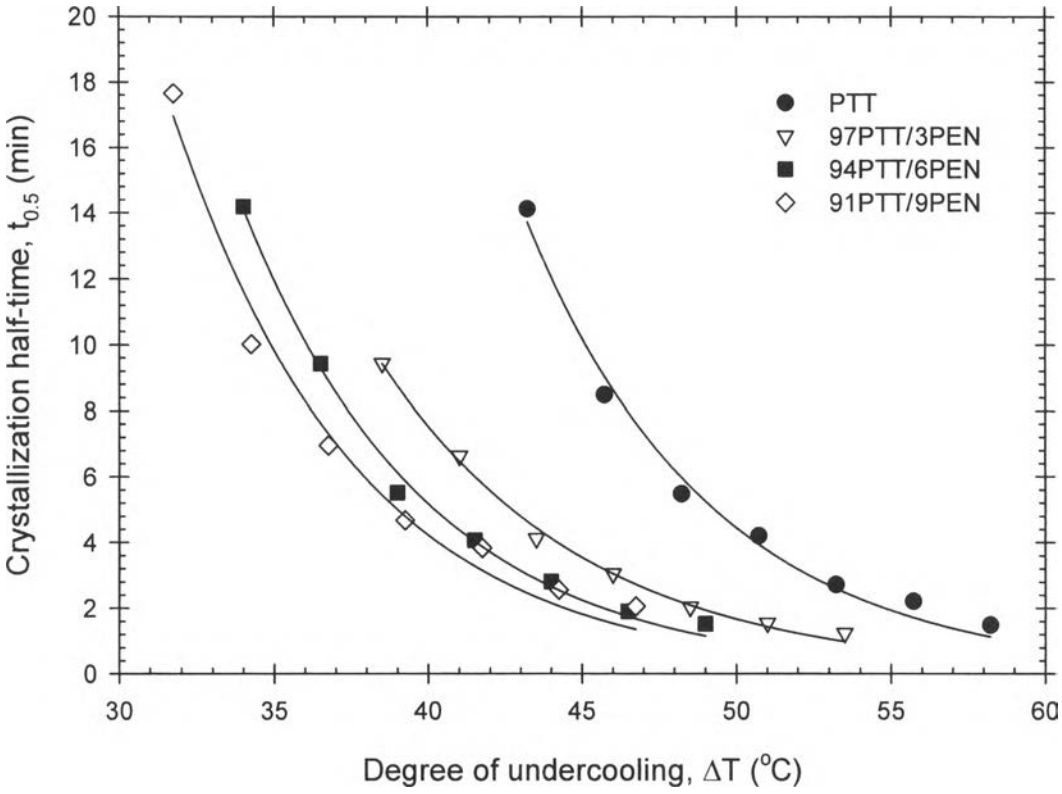
Crystallization half-time, $t_{0.5}$ (min)
Degree of undercooling, ΔT (°C)
PTT
97PTT/3PEN
94PTT/6PEN
91PTT/9PEN
0
2
4
6
8
10
12
14
16
18
20
30
35
40
45
50
55
60

Figure 7.

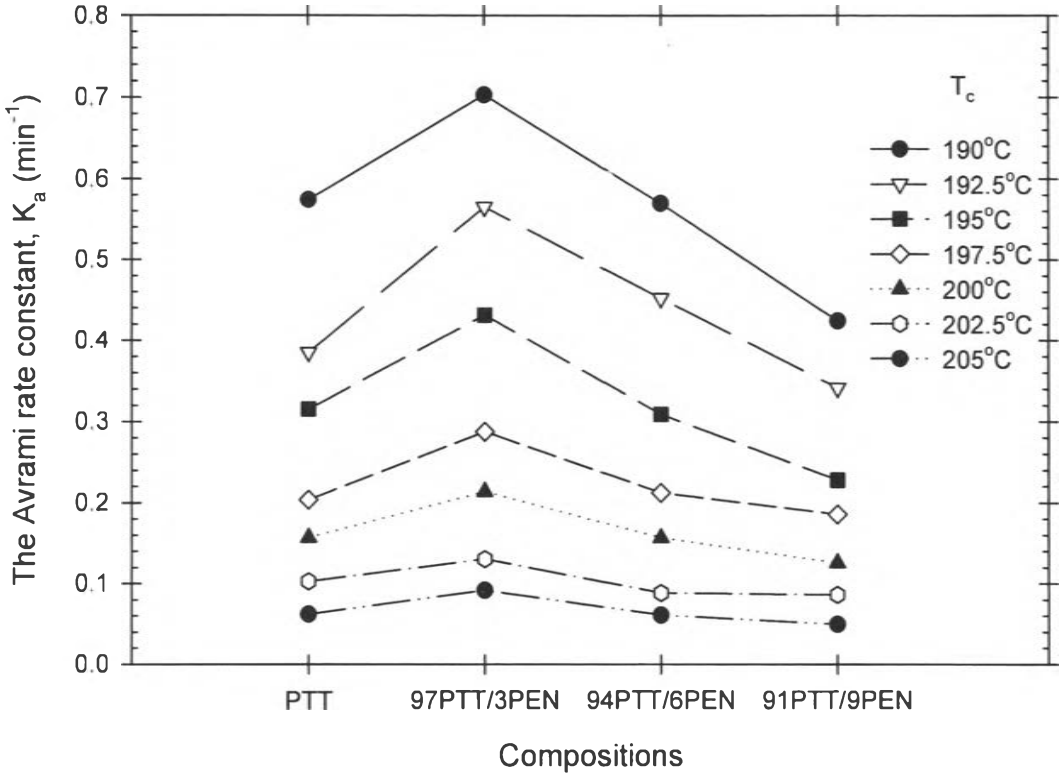
0.8
0.7
0.6
0.5
0.4
0.3
0.2
0.1
0.0
The Avrami rate constant, K_a (min^{-1})
PTT
97PTT/3PEN
94PTT/6PEN
91PTT/9PEN
Compositions
T_c
190°C
192.5°C
195°C
197.5°C
200°C
202.5°C
205°C

Figure 8.

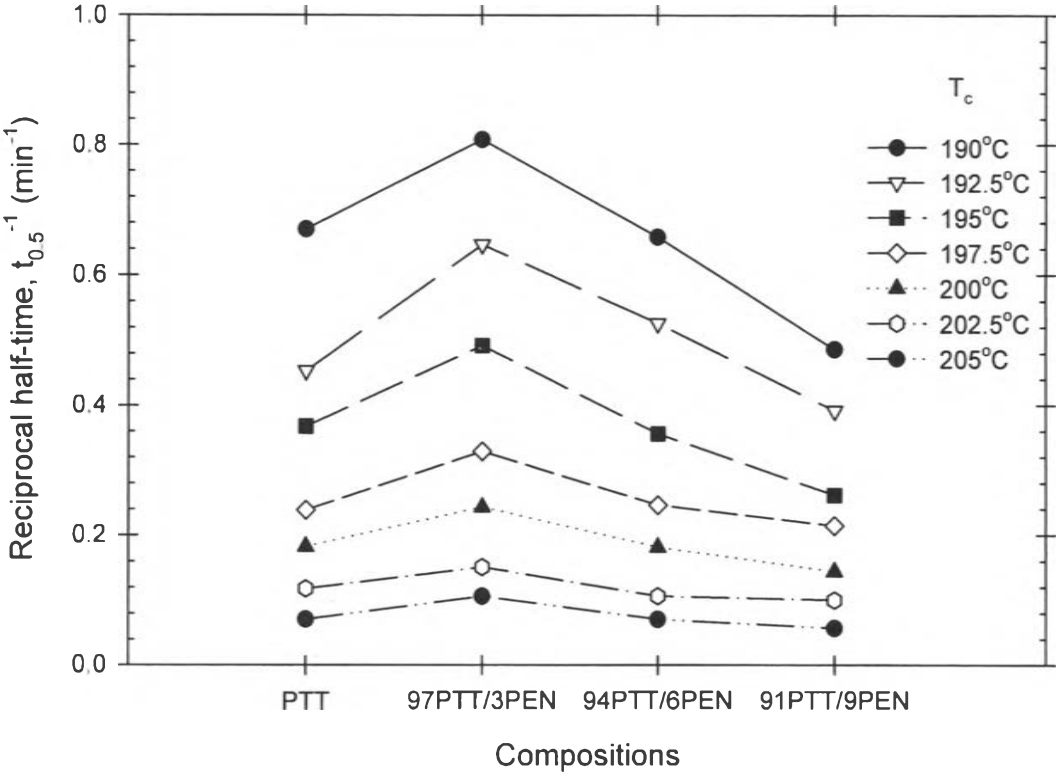
1.0
0.8
0.6
0.4
0.2
0.0
Reciprocal half-time, $t_{0.5}^{-1}$ (min^{-1})
PTT
97PTT/3PEN
94PTT/6PEN
91PTT/9PEN
Compositions
T_c
190°C
192.5°C
195°C
197.5°C
200°C
202.5°C
205°C

Figure 9.

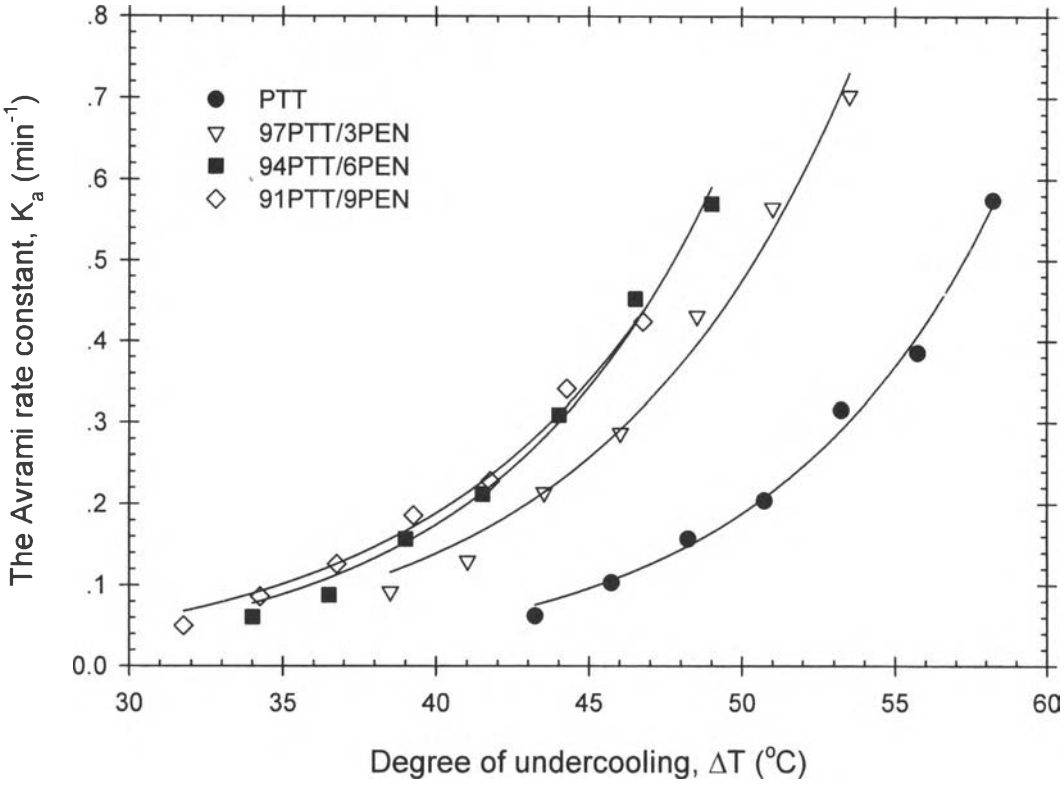
PTT
97PTT/3PEN
94PTT/6PEN
91PTT/9PEN
The Avrami rate constant, K_a (min^{-1})
Degree of undercooling, ΔT (°C)
0.0
.1
.2
.3
.4
.5
.6
.7
.8
30
35
40
45
50
55
60

Figure 10.

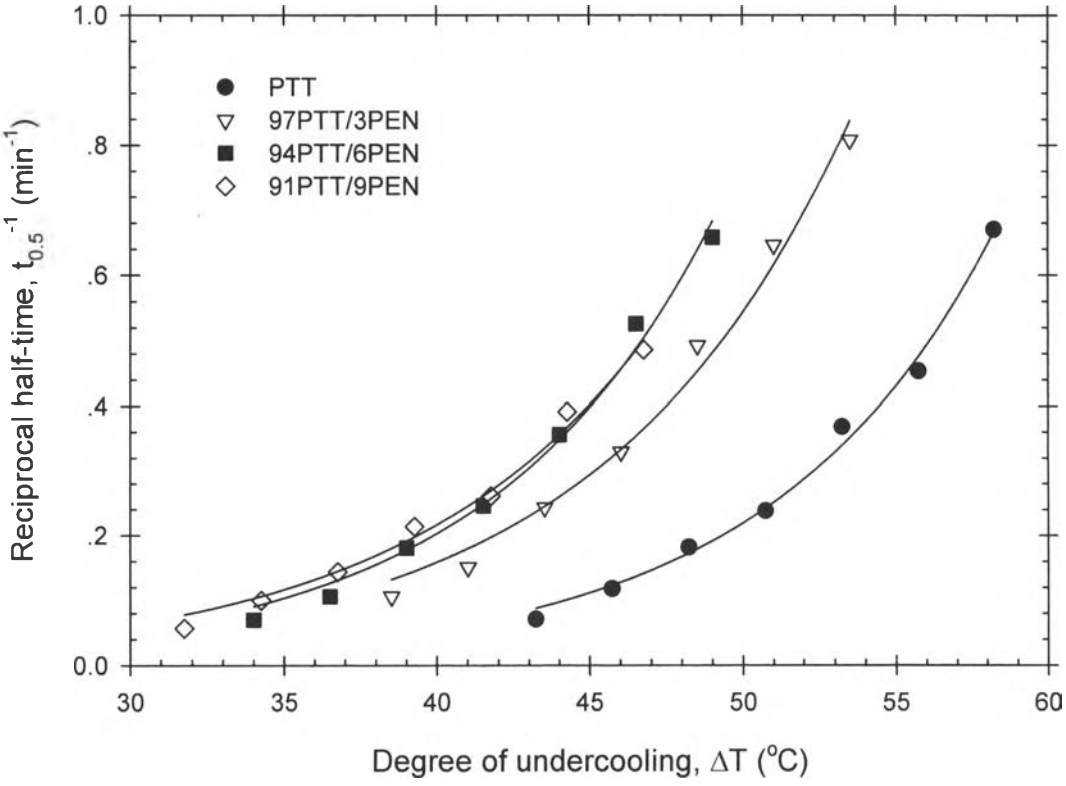
PTT
97PTT/3PEN
94PTT/6PEN
91PTT/9PEN
Reciprocal half-time, $t_{0.5}^{-1}$ (min^{-1})
Degree of undercooling, ΔT (°C)
1.0
.8
.6
.4
.2
0.0
30
35
40
45
50
55
60

Figure 11.

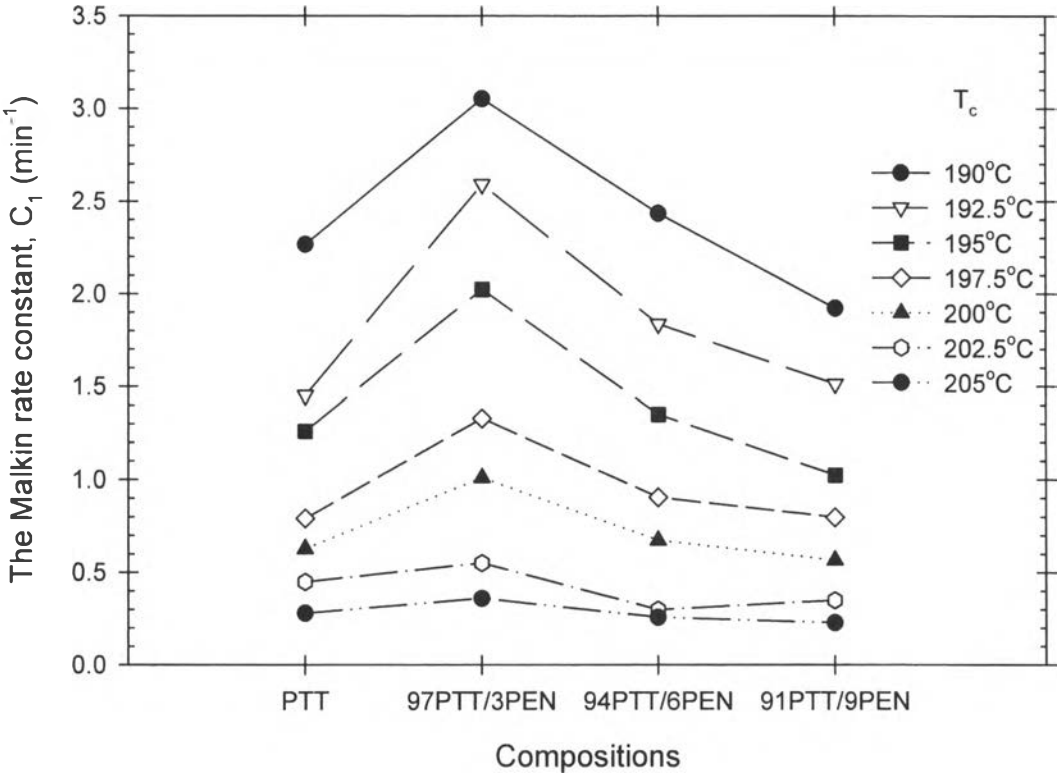
3.5
3.0
2.5
2.0
1.5
1.0
0.5
0.0
The Malkin rate constant, C_1 (min^{-1})
PTT
97PTT/3PEN
94PTT/6PEN
91PTT/9PEN
Compositions
T_c
190°C
192.5°C
195°C
197.5°C
200°C
202.5°C
205°C

Figure 12.

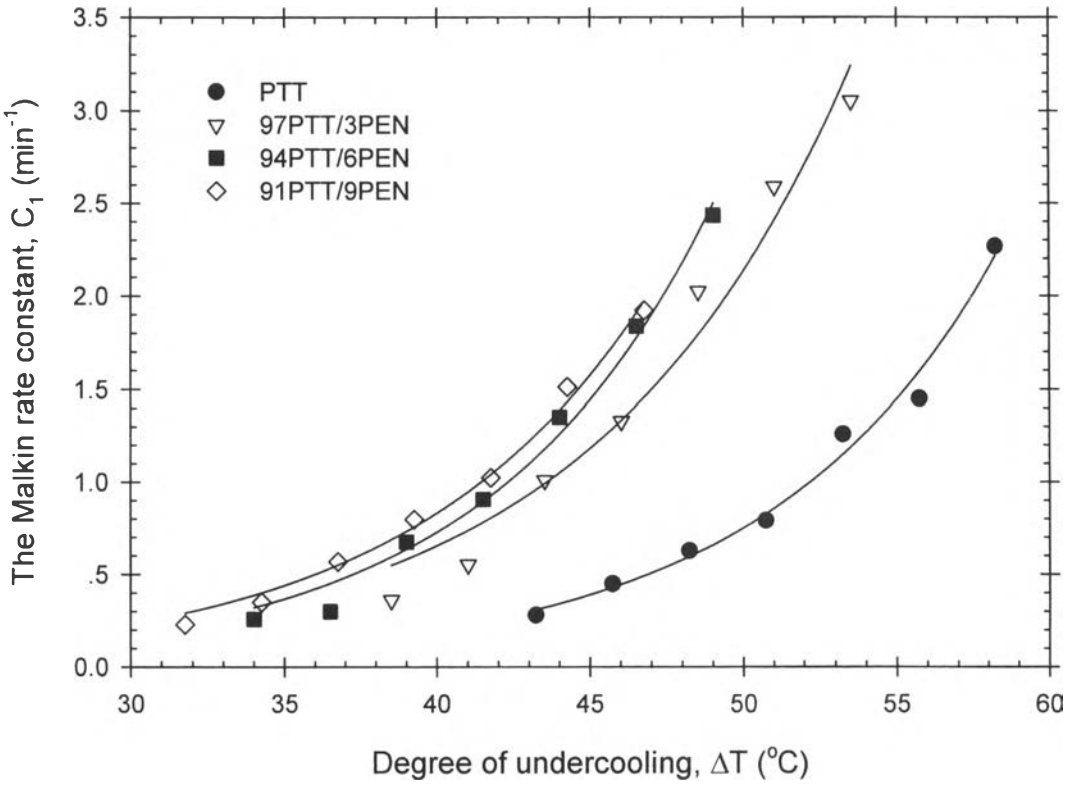

Figure 13.

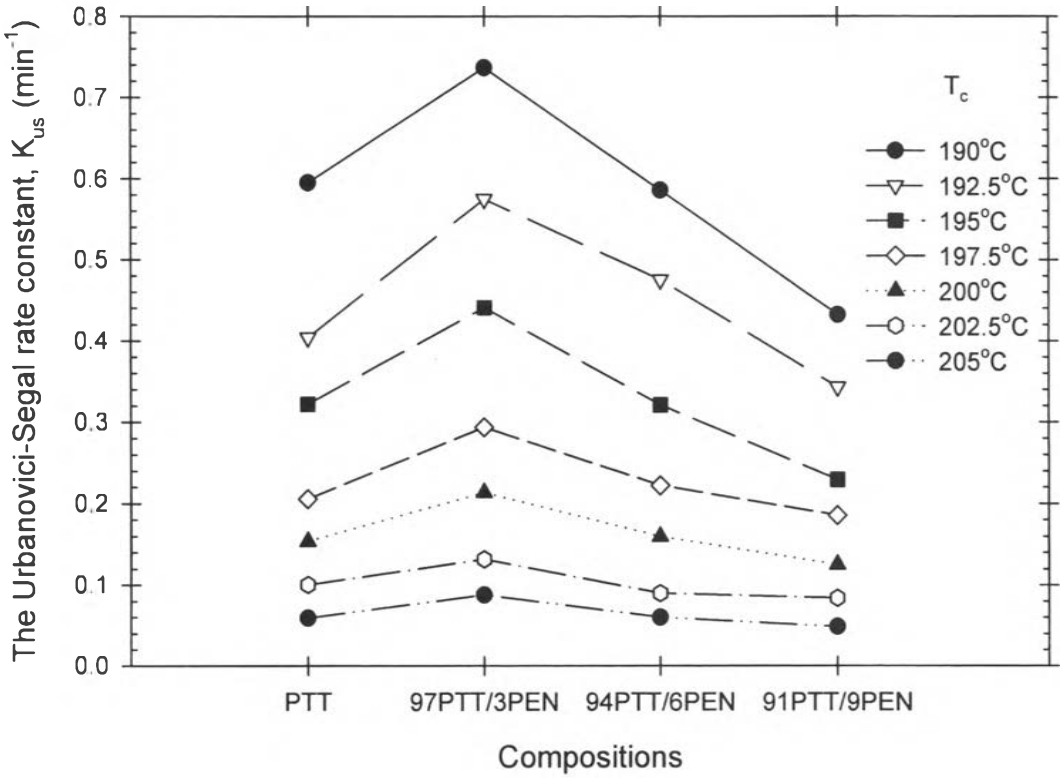
The Urbanovici-Segal rate constant, K_{us} (min^{-1})
0.0
0.1
0.2
0.3
0.4
0.5
0.6
0.7
0.8
PTT
97PTT/3PEN
94PTT/6PEN
91PTT/9PEN
Compositions
T_c
190°C
192.5°C
195°C
197.5°C
200°C
202.5°C
205°C

Figure 14.

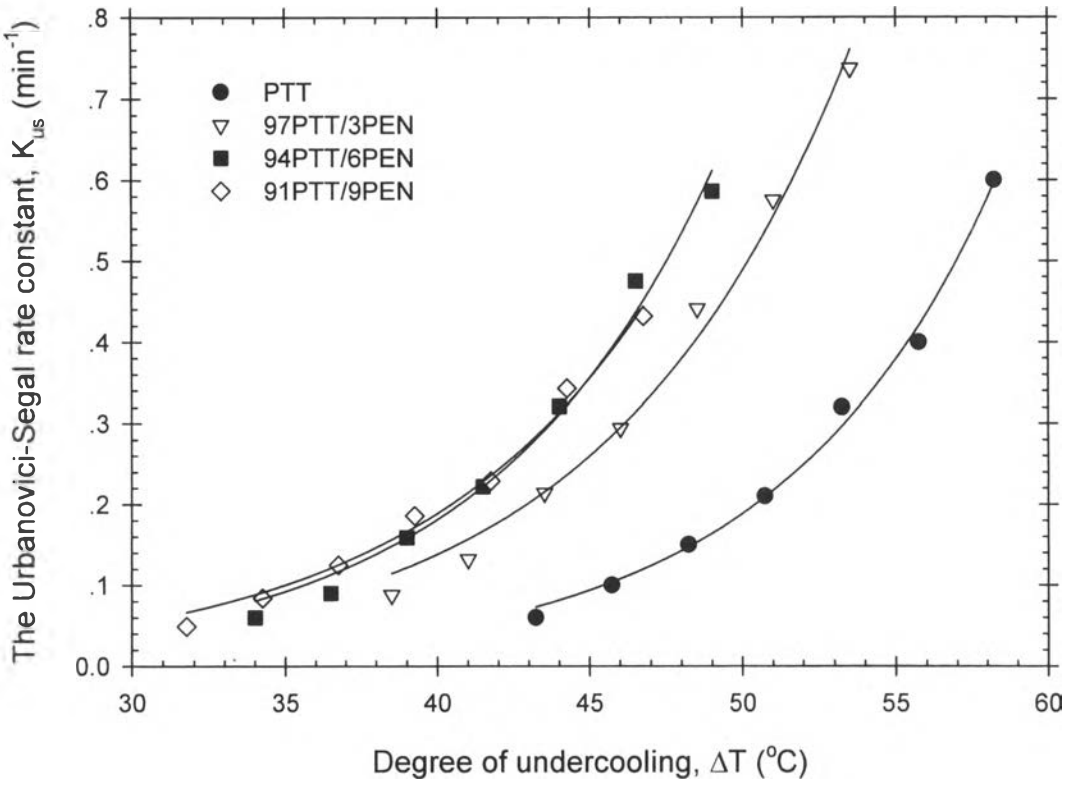
PTT
97PTT/3PEN
94PTT/6PEN
91PTT/9PEN
The Urbanovici-Segal rate constant, K_{US} (min^{-1})
Degree of undercooling, ΔT (°C)
0.0
.1
.2
.3
.4
.5
.6
.7
.8
30
35
40
45
50
55
60

Figure 15.

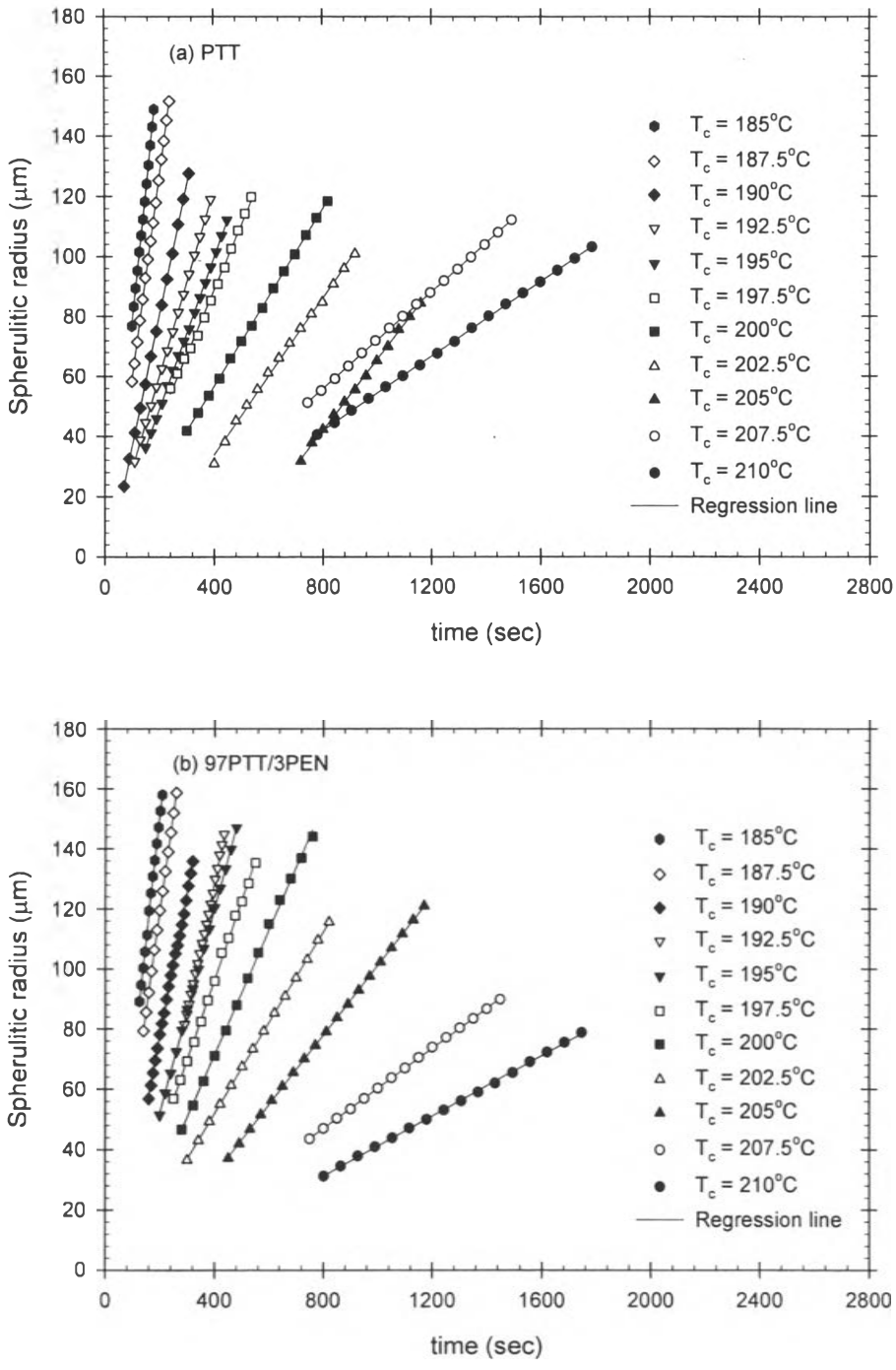
(a) PTT
Spherulitic radius (μm)
time (sec)
T_c = 185°C
T_c = 187.5°C
T_c = 190°C
T_c = 192.5°C
T_c = 195°C
T_c = 197.5°C
T_c = 200°C
T_c = 202.5°C
T_c = 205°C
T_c = 207.5°C
T_c = 210°C
Regression line
(b) 97PTT/3PEN
Spherulitic radius (μm)
time (sec)
T_c = 185°C
T_c = 187.5°C
T_c = 190°C
T_c = 192.5°C
T_c = 195°C
T_c = 197.5°C
T_c = 200°C
T_c = 202.5°C
T_c = 205°C
T_c = 207.5°C
T_c = 210°C
Regression line

Figure 16.

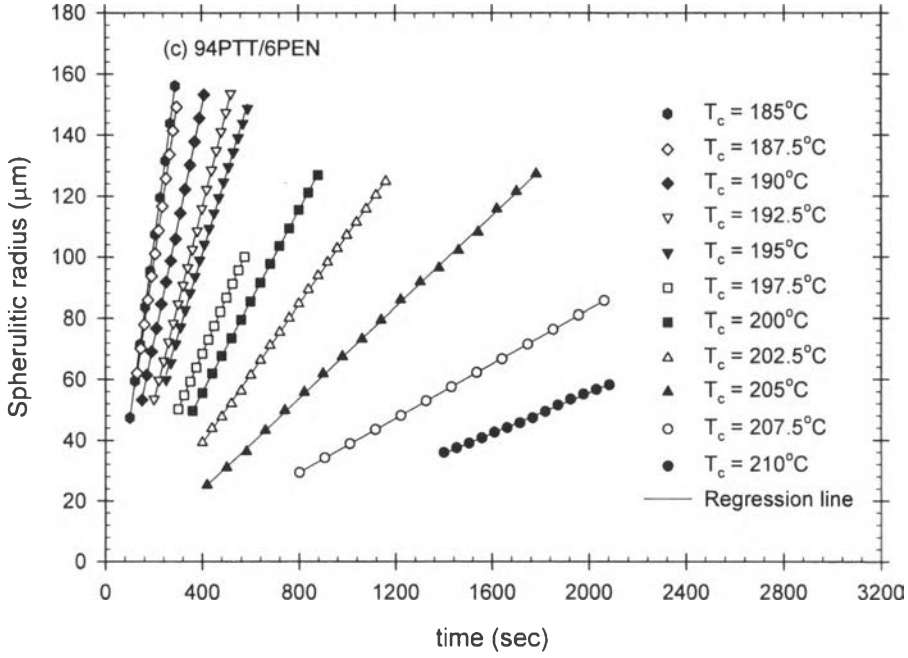

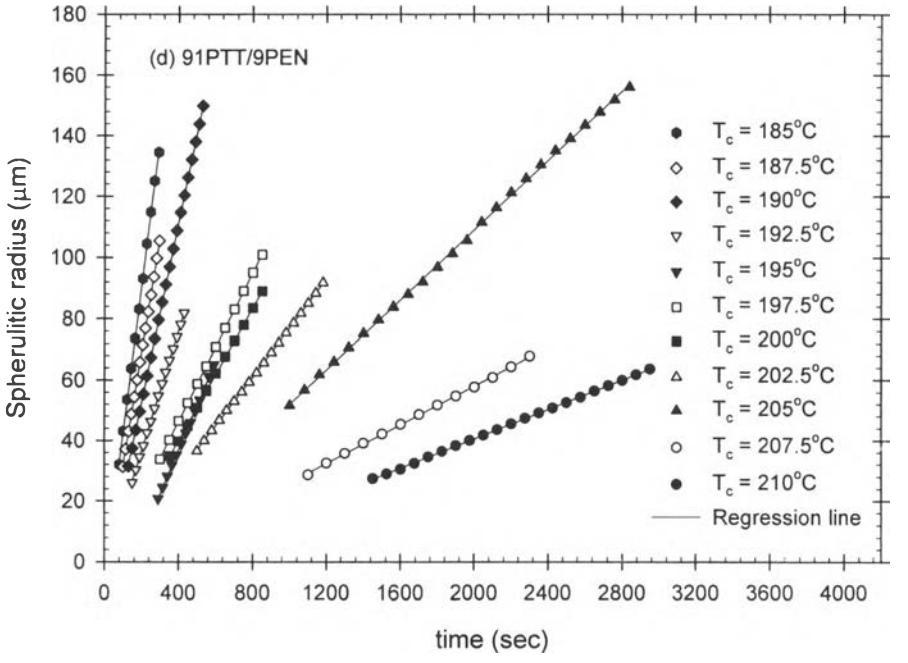

Figure 16. (continued)

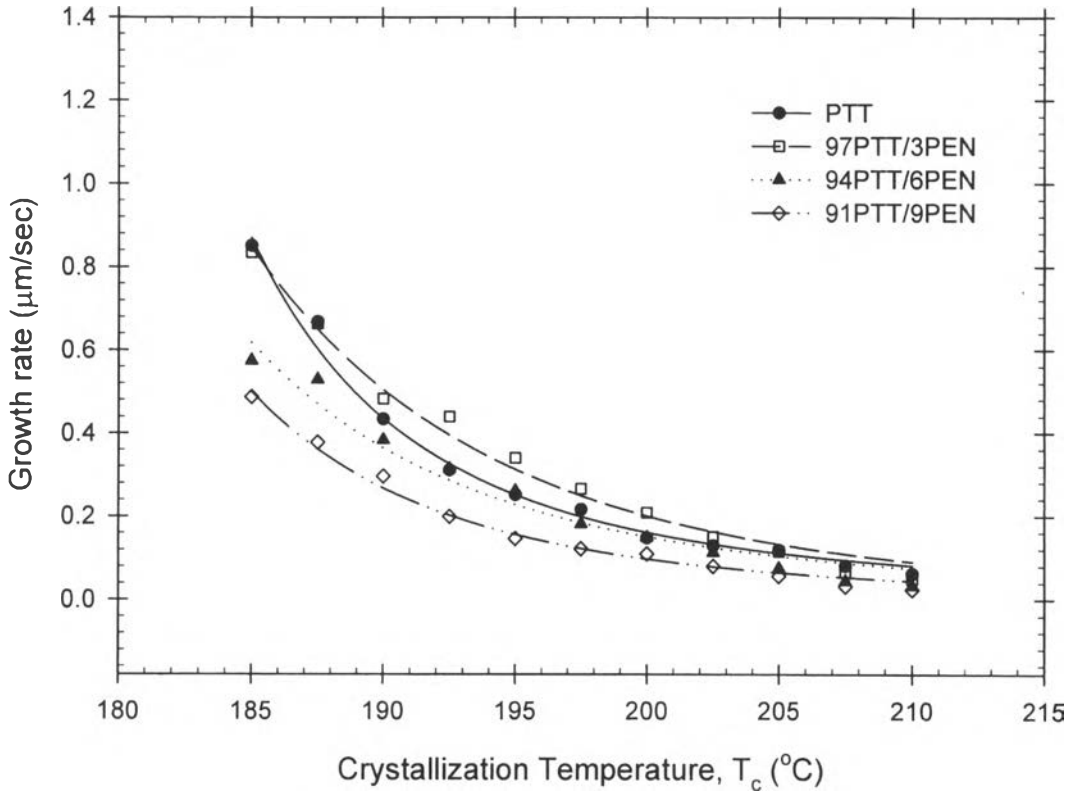
1.4
1.2
1.0
0.8
0.6
0.4
0.2
0.0
Growth rate (μm/sec)
180
185
190
195
200
205
210
215
Crystallization Temperature, T_c (°C)
PTT
97PTT/3PEN
94PTT/6PEN
91PTT/9PEN

Figure 17.

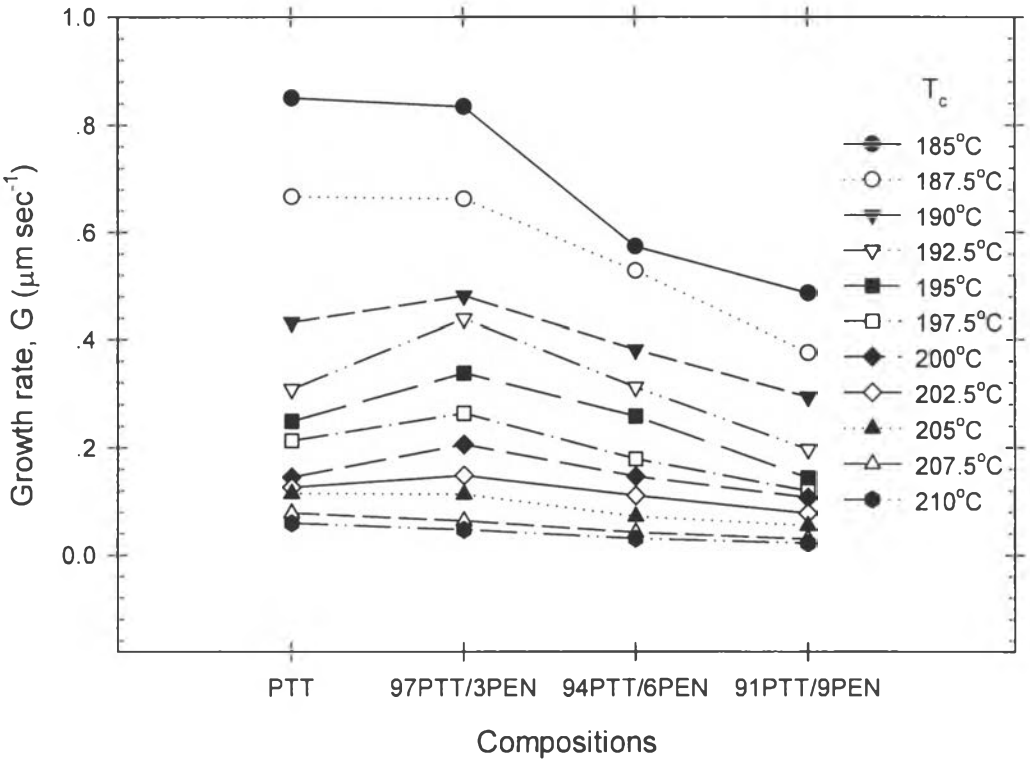
1.0
.8
.6
.4
.2
0.0
Growth rate, G (μm sec-1)
PTT
97PTT/3PEN
94PTT/6PEN
91PTT/9PEN
Compositions
Tc
185°C
187.5°C
190°C
192.5°C
195°C
197.5°C
200°C
202.5°C
205°C
207.5°C
210°C

Figure 18.

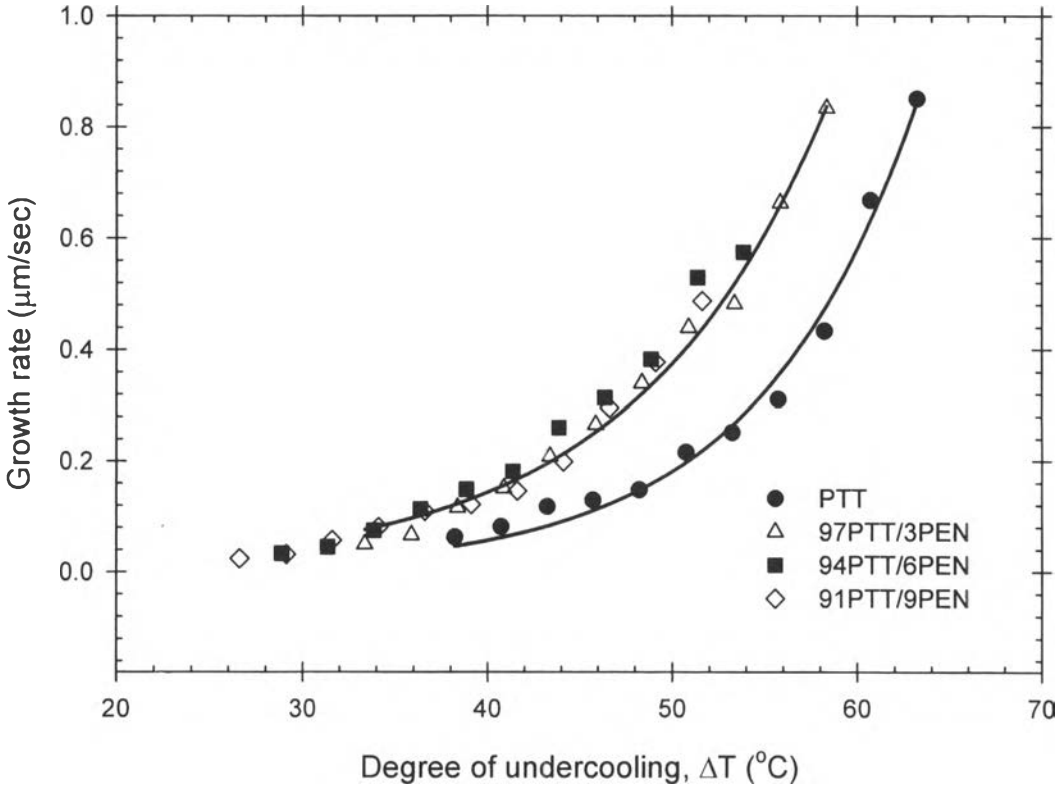
1.0
0.8
0.6
0.4
0.2
0.0
Growth rate (μm/sec)
20
30
40
50
60
70
Degree of undercooling, ΔT (°C)
PTT
97PTT/3PEN
94PTT/6PEN
91PTT/9PEN

Figure 19.

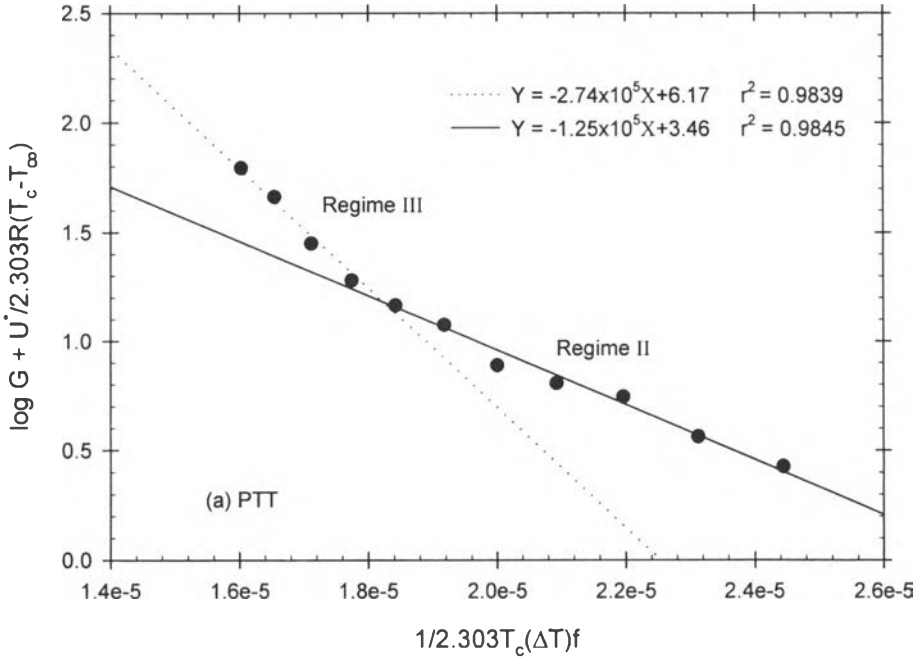
Y = -2.74x10^5X+6.17 r^2 = 0.9839
Y = -1.25x10^5X+3.46 r^2 = 0.9845
Regime III
Regime II
(a) PTT
log G + U*/2.303R(T_c-T_∞)
1/2.303T_c(ΔT)f
2.5
2.0
1.5
1.0
0.5
0.0
1.4e-5
1.6e-5
1.8e-5
2.0e-5
2.2e-5
2.4e-5
2.6e-5

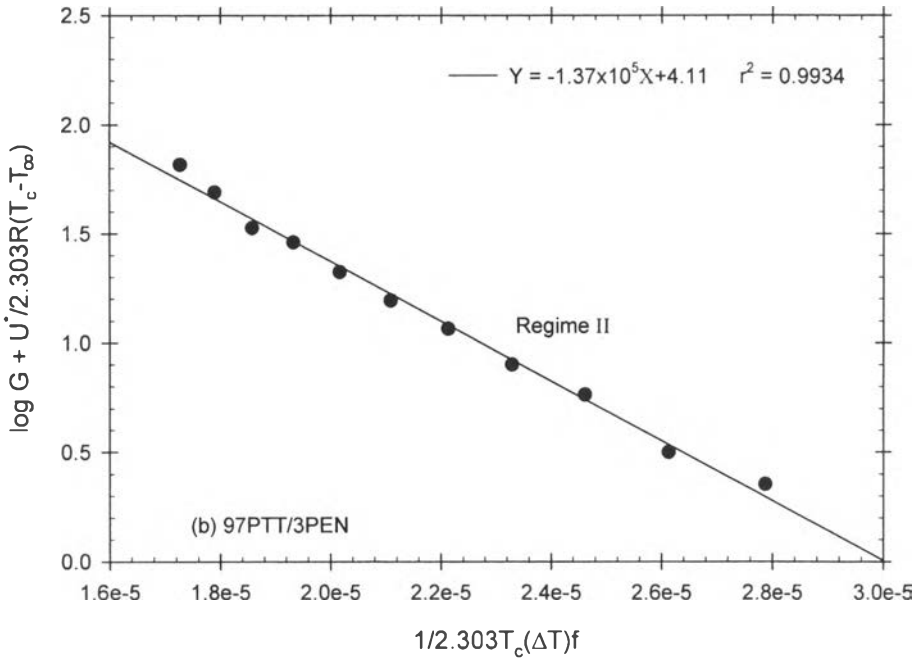
Y = -1.37x10^5X+4.11 r^2 = 0.9934
Regime II
(b) 97PTT/3PEN
log G + U*/2.303R(T_c-T_∞)
1/2.303T_c(ΔT)f
2.5
2.0
1.5
1.0
0.5
0.0
1.6e-5
1.8e-5
2.0e-5
2.2e-5
2.4e-5
2.6e-5
2.8e-5
3.0e-5

Figure 20.

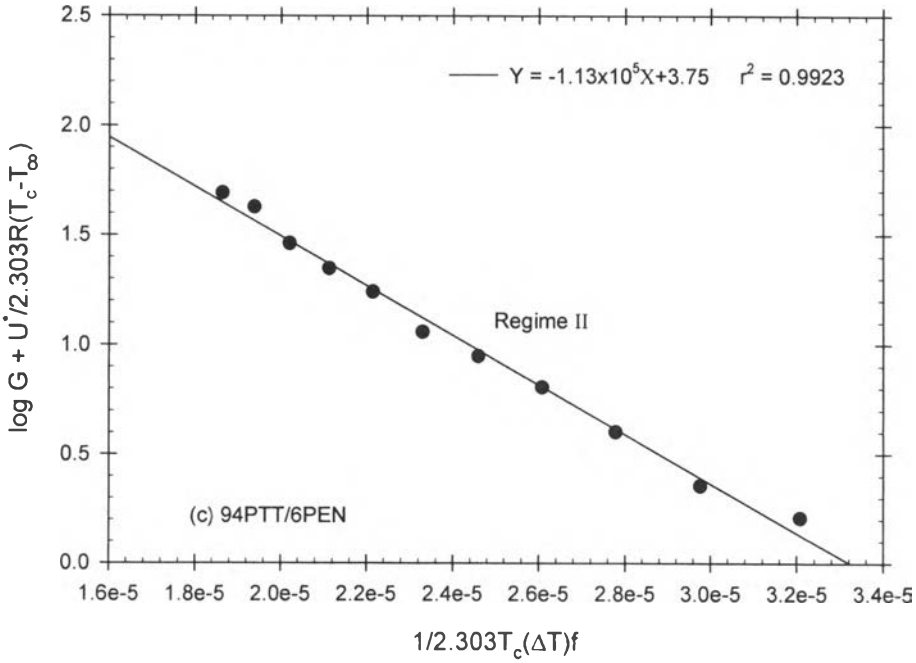

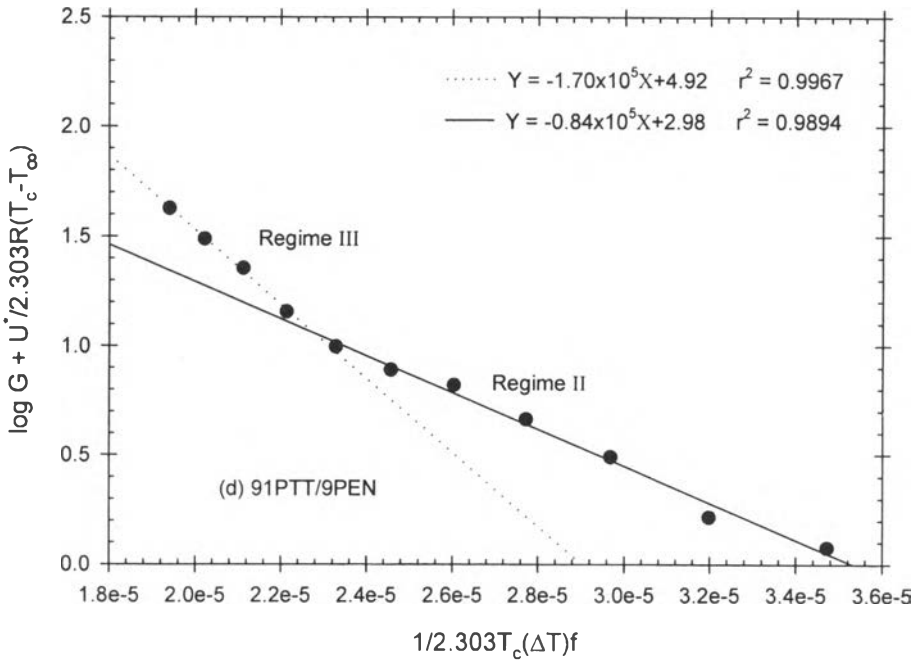

Figure 20. (continued)

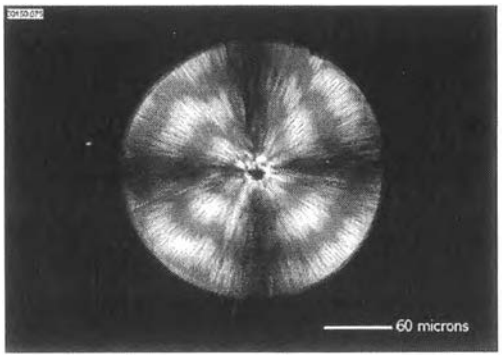

(a) 185°C

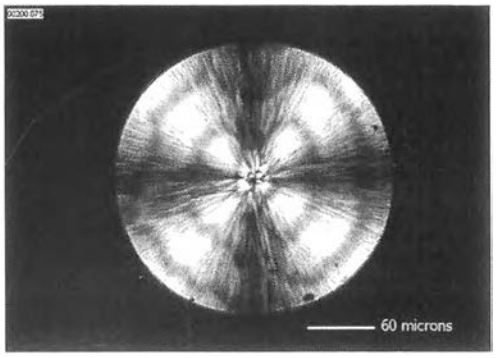

(b) 187.5°C

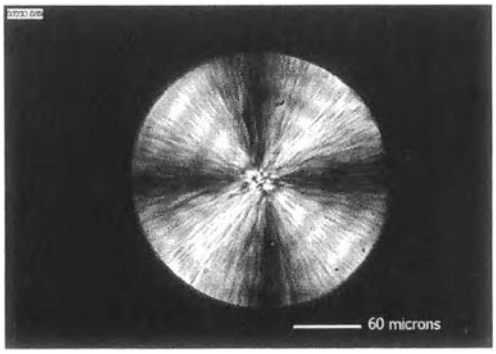

(c) 190°C

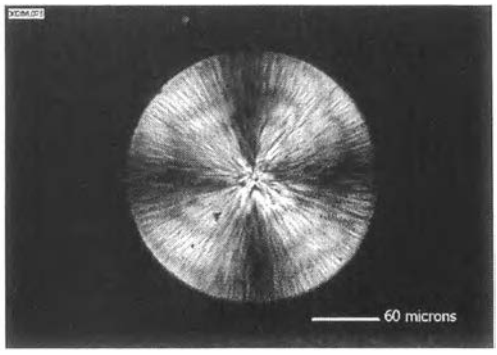

(d) 192.5°C

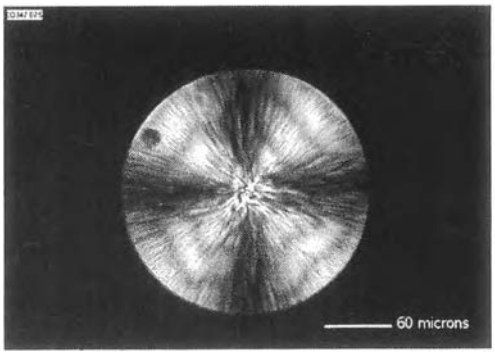

(e) 195°C

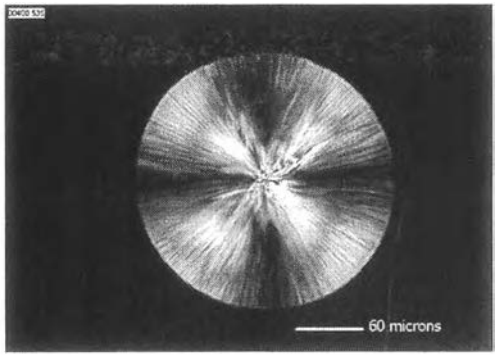

(f) 197.5°C

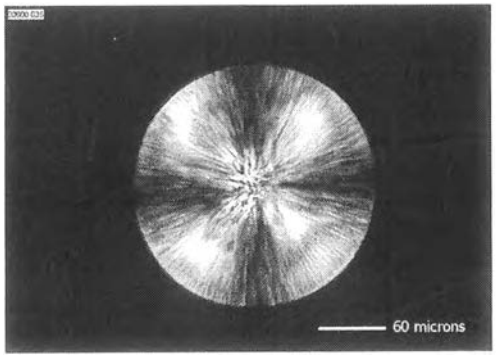

(g) 200°C

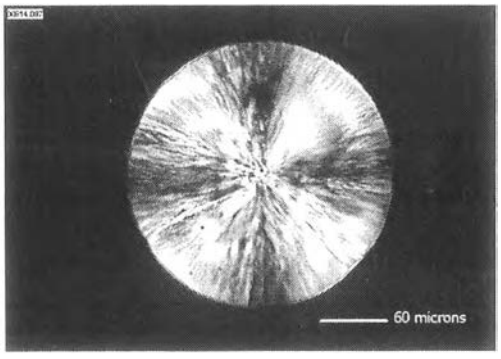

(h) 202.5°C

Figure 21.

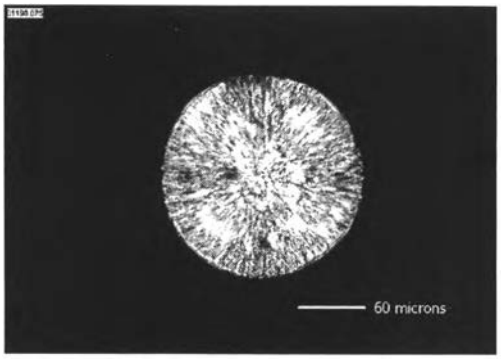

(i) 205°C

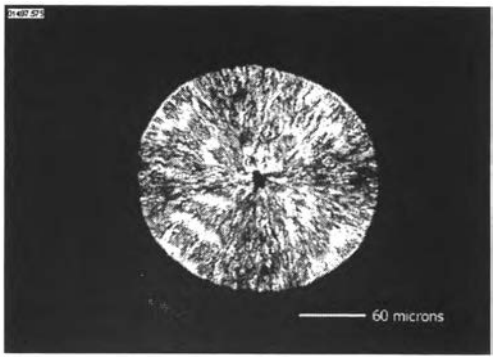

(j) 207.5°C

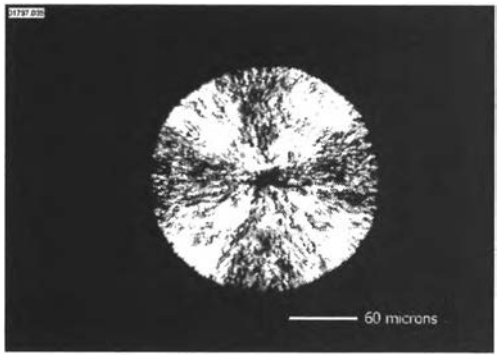

(k) 210°C

Figure 21. (continued)

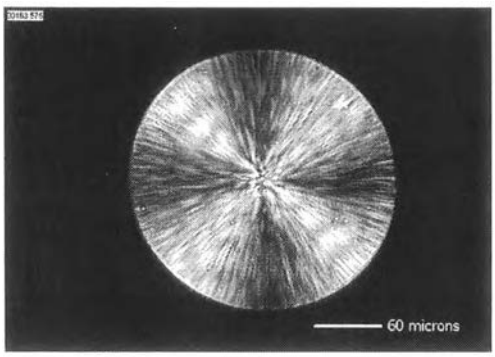

(a) 185°C

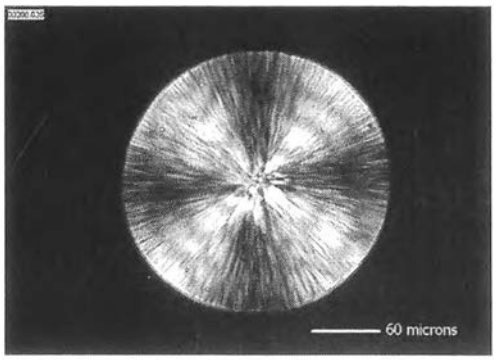

(b) 187.5°C

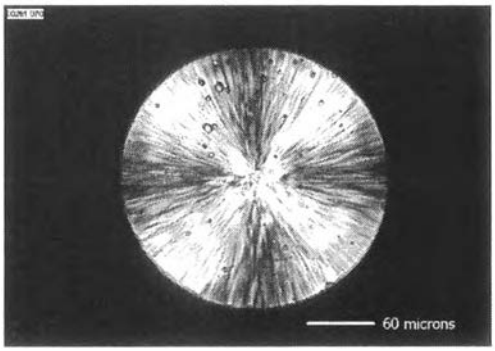

(c) 190°C

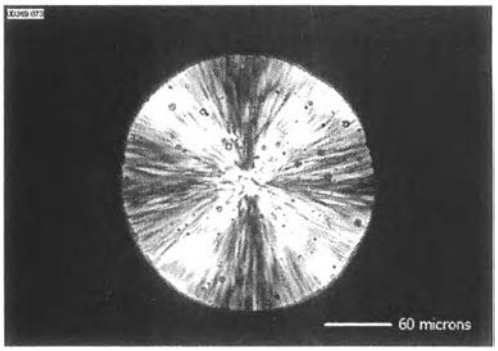

(d) 192.5°C

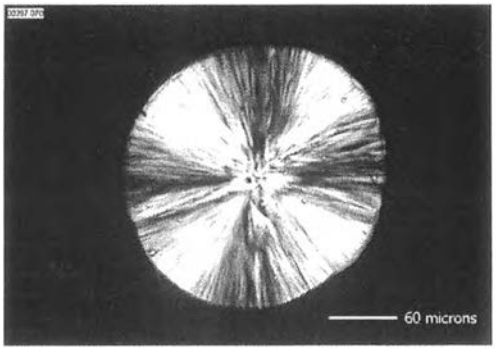

(e) 195°C

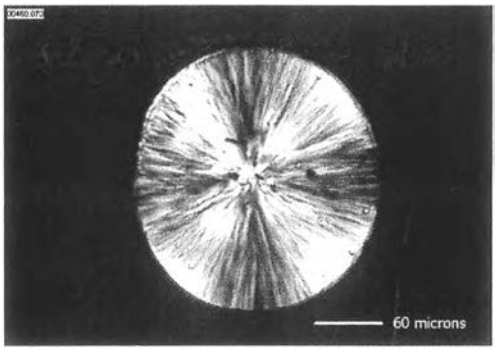

(f) 197.5°C

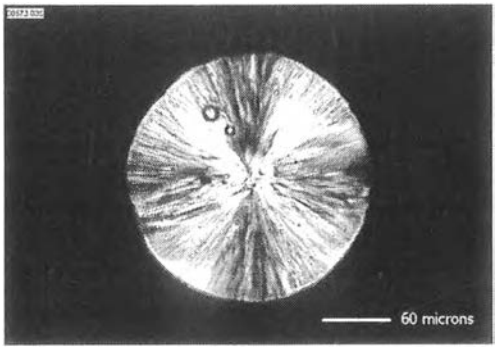

(g) 200°C

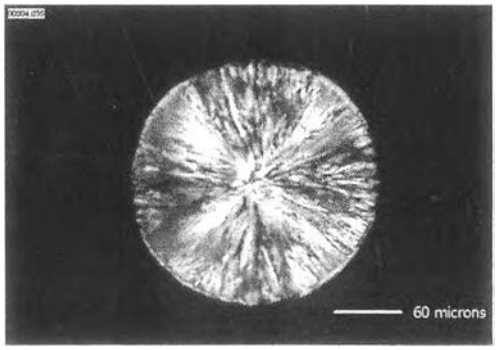

(h) 202.5°C

Figure 22.

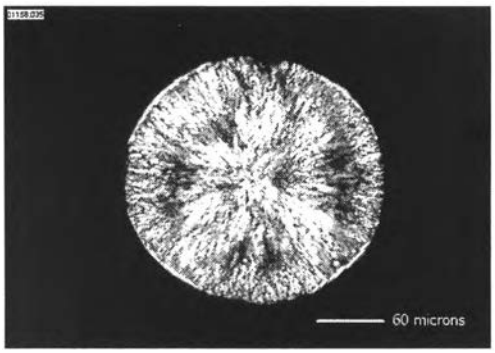

(i) 205°C

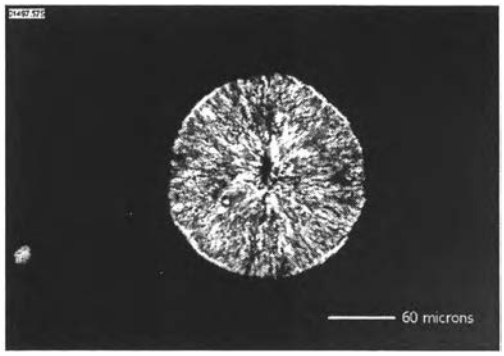

(j) 207.5°C

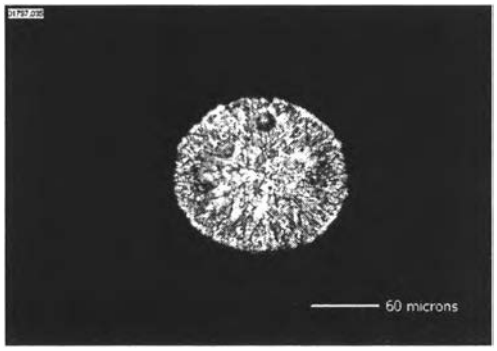

(k) 210°C

Figure 22. (continued)

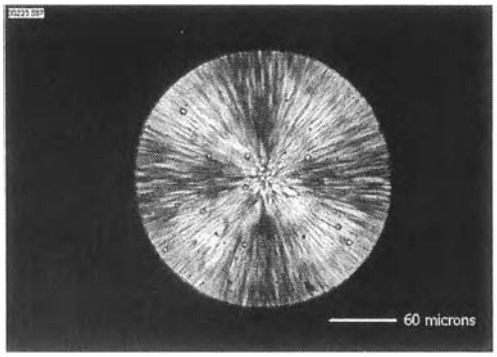

(a) 185°C

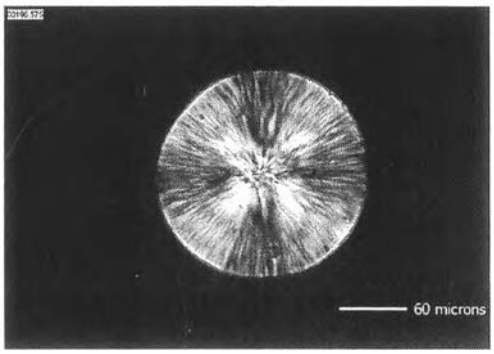

(b) 187.5°C

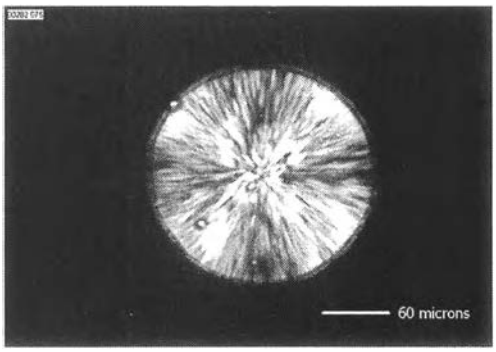

(c) 190°C

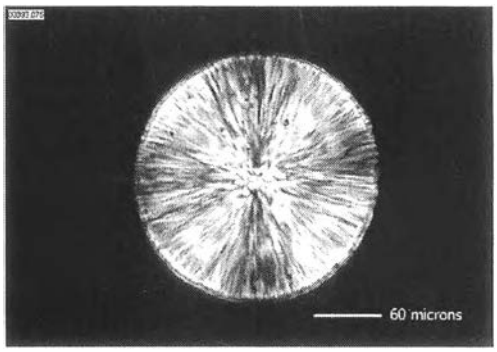

(d) 192.5°C

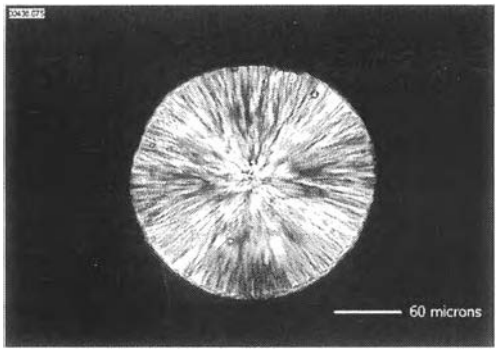

(e) 195°C

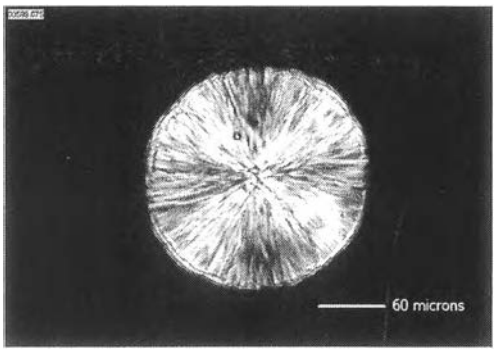

(f) 197.5°C

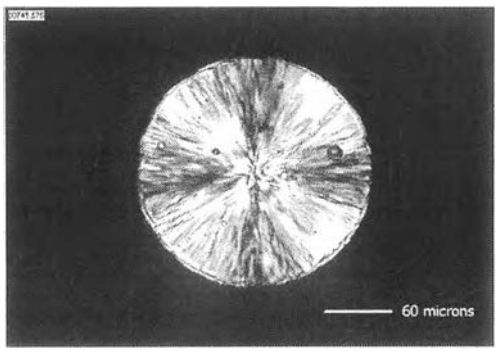

(g) 200°C

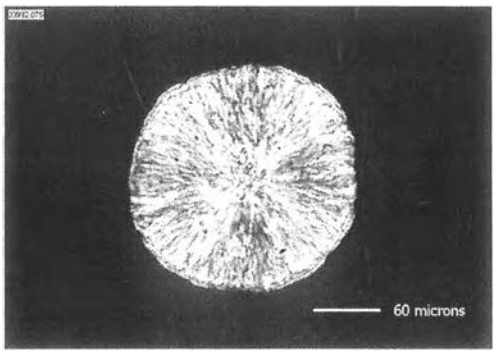

(h) 202.5°C

Figure 23.

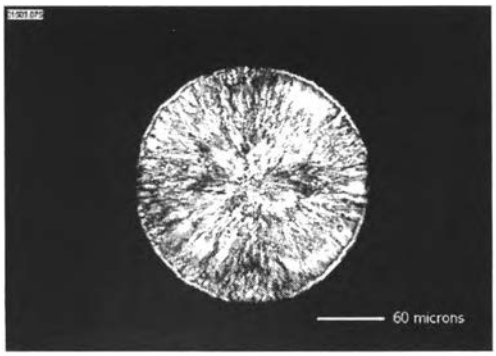

(i) 205°C

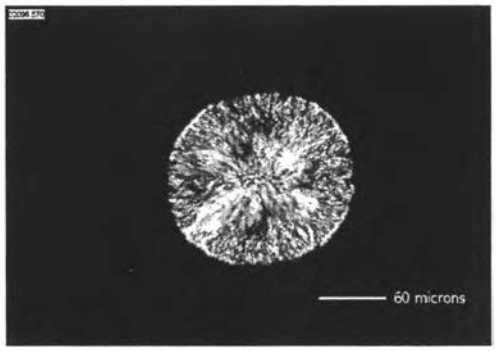

(j) 207.5°C

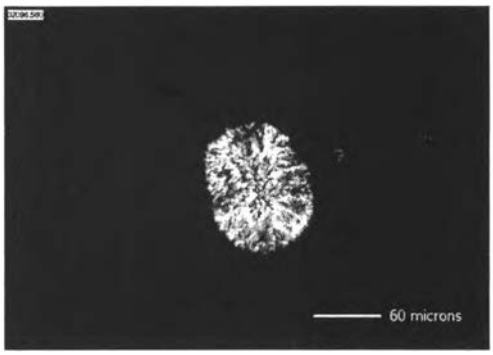

(k) 210°C

Figure 23. (continued)

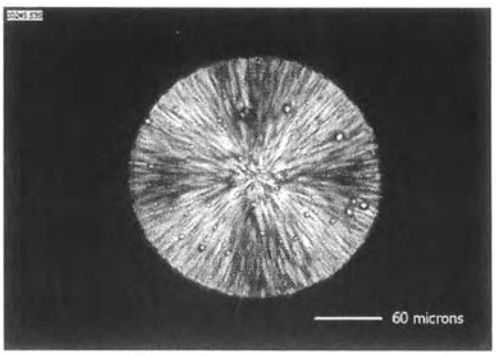

(a) 185°C

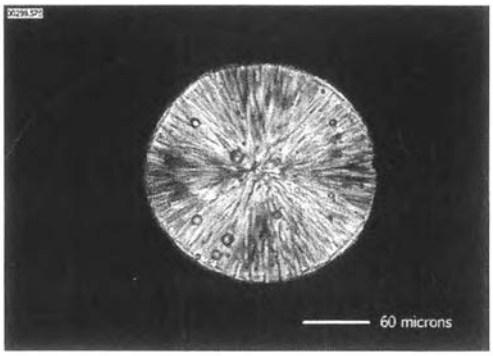

(b) 187.5°C

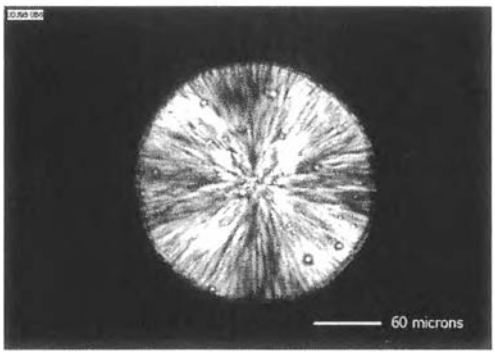

(c) 190°C

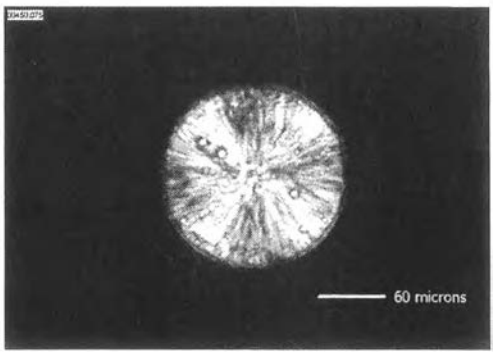

(d) 192.5°C

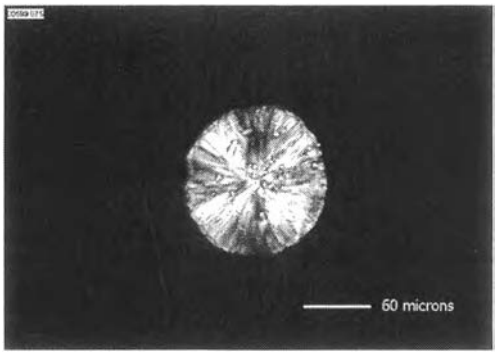

(e) 195°C

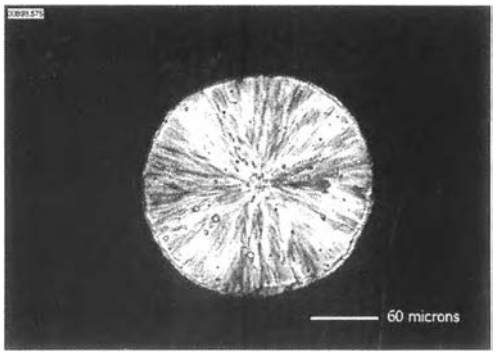

(f) 197.5°C

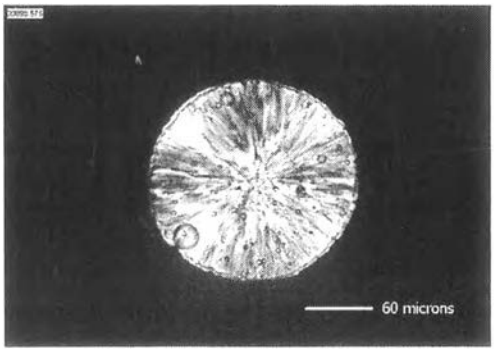

(g) 200°C

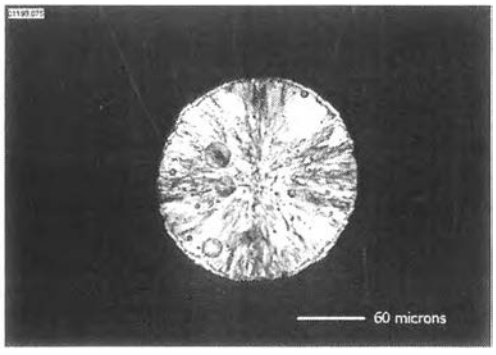

(h) 202.5°C

Figure 24.

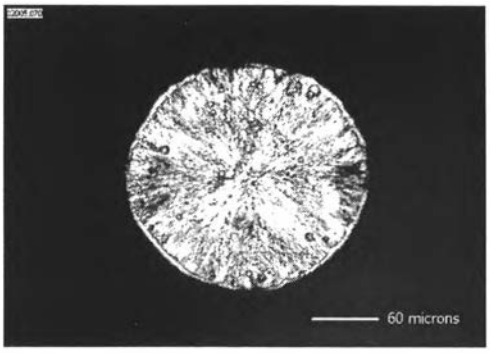

(i) 205°C

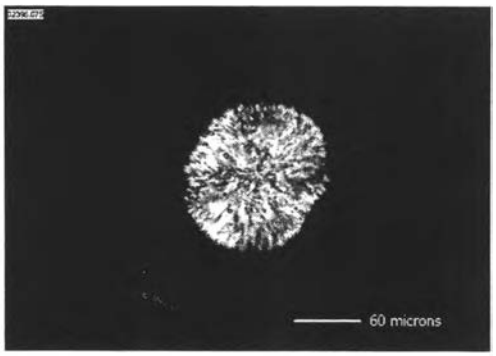

(j) 207.5°C

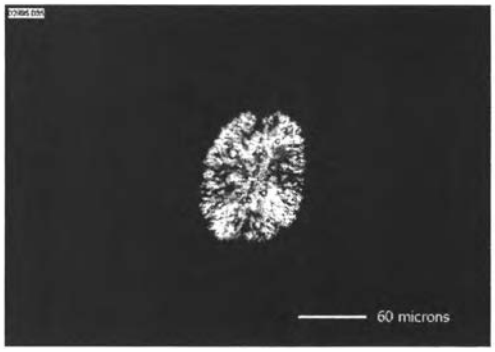

(k) 210°C

Figure 24. (continued)

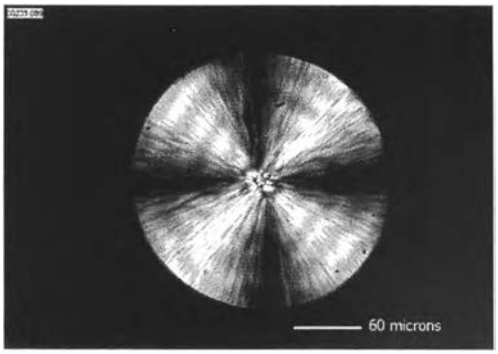

(a) PTT

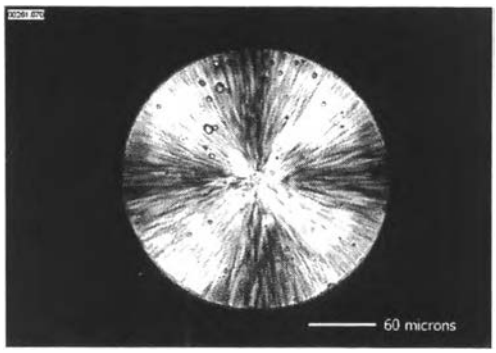

(b) 97PTT/3PEN

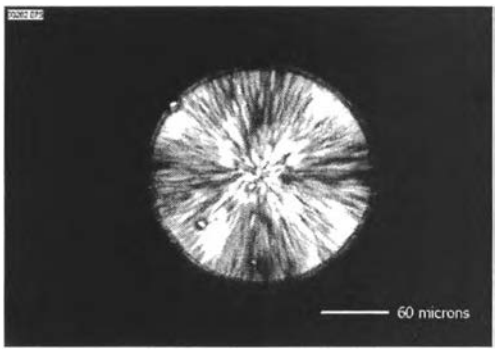

(c) 94PTT/6PEN

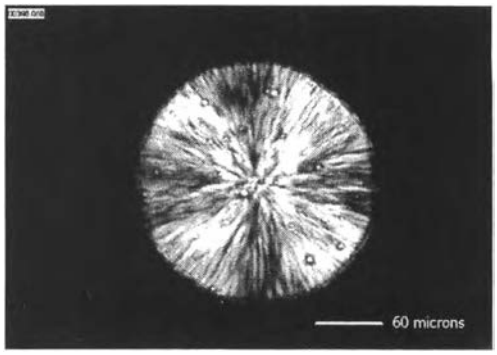

(d) 91PTT/9PEN

Figure 25.

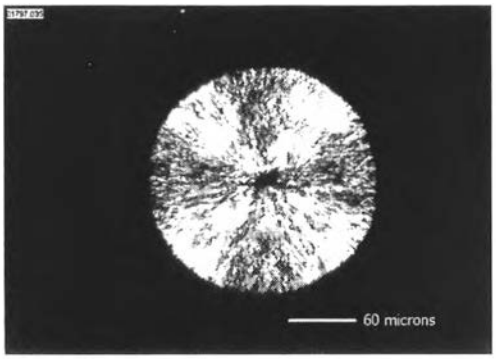

(a) PTT

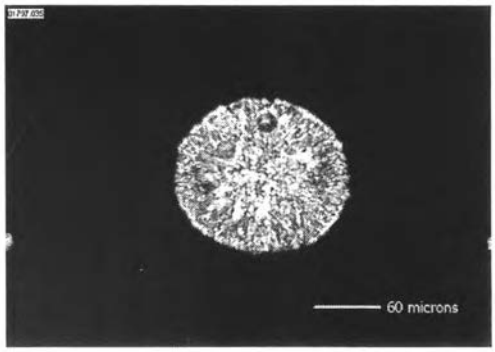

(b) 97PTT/3PEN

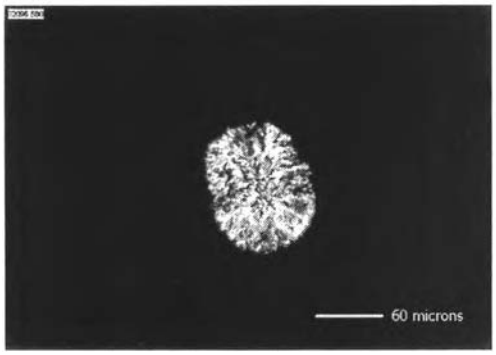

(c) 94PTT/6PEN

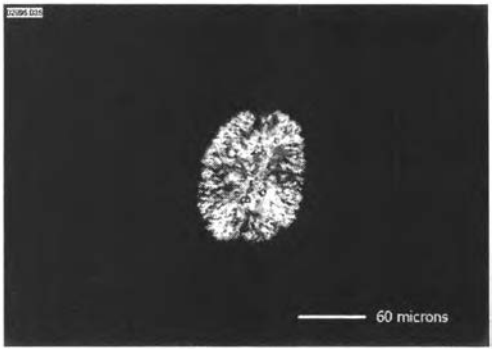

(d) 91PTT/9PEN

Figure 26.

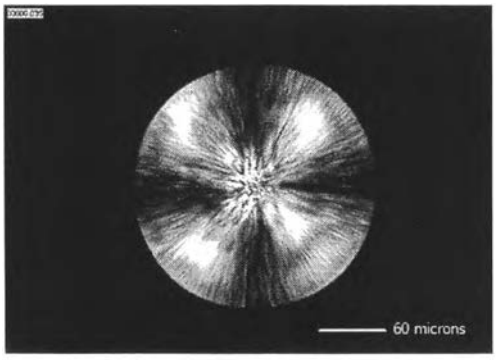

(a) PTT

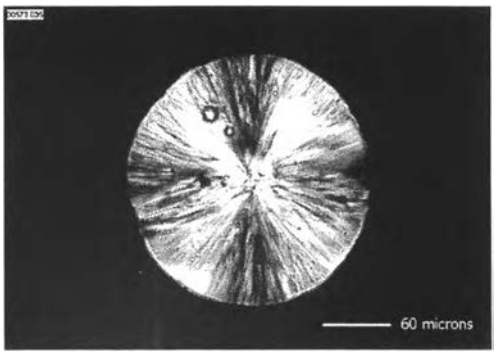

(b) 97PTT/3PEN

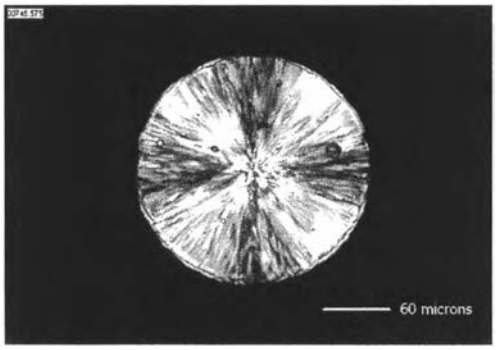

(c) 94PTT/6PEN

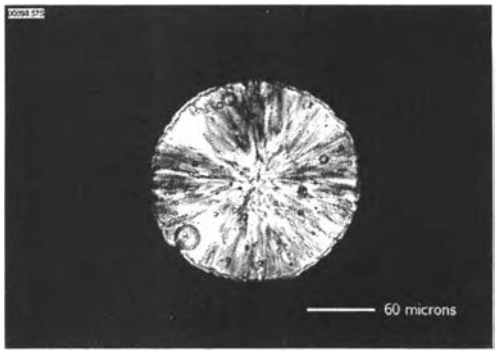

(d) 91PTT/9PEN

Figure 27.